

45. THE INFLUENCE OF SEDIMENT COMPOSITION ON PHYSICAL PROPERTIES INTERRELATIONSHIPS¹

Ulf Bayer, Institut für Geologie und Paläontologie, Universität Tübingen, Tübingen, Federal Republic of Germany

ABSTRACT

Physical properties measured in Mesozoic to Recent sediments at DSDP Sites 511–514 are summarized, compared, and related to sedimentological composition. Lithification in clays and nannofossil oozes starts at porosities of less than 60% and affects sonic velocity very strongly, whereas compaction causes little increase in sonic velocity. Shear strength increases rapidly with decreasing porosity within all observed lithologies (clays, nannofossil, and diatomaceous oozes). In diatomaceous oozes and muds the stress–strain relationship of the vane shear test depends on the anisotropic properties of the sediment. Within Tertiary and younger sediments, physical properties other than shear strength depend much more on sedimentological composition than on compaction, which is measured from the porosity data. The physical properties data are viewed as the output of the developing sediment “system” and are related through simple interaction models.

INTRODUCTION

Measurement of the physical properties of sediments is a well-established, routine procedure aboard *Glomar Challenger*. In previous DSDP reports, the different methods are well described, notably by Boyce (1976a, 1977). So too are the general problems associated with physical property measurements in conventionally cored material (Bennett and Keller, 1973; Demars et al., 1979; von Huene et al., 1973).

During Leg 71 the relatively new Serocki–Storms–Cameron hydraulic piston corer was used at two sites. Most of the cores were well preserved (see site chapters for Sites 512, 514); nevertheless, there is evidence that physical properties may be remarkably disturbed even in piston cores. In very soft sediments, flow-in commonly occurred, whereas in stiff sediments the build-up of internal pressure during coring caused fracturing of the plastic tube and artificial compaction of the sediment.

In this chapter, all Leg 71 physical property data are summarized, and an attempt is made to compare them as well as to relate them to the sedimentological data summarized in the site chapters. Physical properties may be viewed from different perspectives. Their practical use in seismic and engineering work leads to a static view in which physical properties are treated as “physical constants” for a certain lithological unit or are related to empirically useful parameters such as sub-bottom depth (e.g., Hamilton, 1976a–d, 1978, 1979; Bachman and Hamilton, 1976; Keller, 1974; Lee, 1973).

Alternatively, physical properties can be viewed as the momentary measurable output of the sediment system that is developing through the action of complex physical and chemical processes. These processes can be subdivided into a group of initial conditions—sediment composition, texture, or stratification—and into time-

dependent historical processes, such as burial resulting in compaction, or diagenesis. Finally, the system may be disturbed by occasional events, like the entry of basaltic sills into the sediment (Einsele, 1982). Although the Leg 71 data cover only a small range of possible physical property values, this chapter attempts to view physical properties and sedimentology as dynamically interactive systems.

METHODS

Water Content, Bulk Density, Porosity, and Grain Density

The continuous GRAPE was run for all cores during Leg 71. For this analysis, however, only values determined by gravimetric methods (Boyce, 1976a) have been used. *Bulk density* and *water content* are related to the wet weight of the samples; that is, they are defined as “wet-bulk density” (g/cm^3) and “wet water content” (fractions or percentages). The volume of samples was measured for chunks weighed in air and under water and, where the sediment was soft enough, by taking cylinder samples of known volume. Both methods were alternated to check for systematic errors. All samples that I took were processed immediately after they were taken.

Water content and *porosity* were calculated from the water loss at 110°C. *Grain density* was computed from the wet-bulk density data and the porosity data. The porosity data were computed on the assumption that the sediments were water-saturated. The computed grain density data were used mainly to test the validity of the other mass physical property data. Using this test, only very few sets of data had to be rejected; most of the rejected samples had been fractured considerably during sampling. No corrections for salt content (e.g., Boyce, 1976a) or for elastic rebound (Hamilton, 1976, Einsele, 1982) were incorporated in the results.

Shrinkage

Shrinkage values were estimated from the cylinder samples. Shrinkage (*sh*) is the loss of volume expressed as a percentage of the original volume V_o , after wet cylinder samples have been dried at 110°C (see Einsele, 1982):

$$sh = \frac{V_o - V_s}{V_o}$$

The volume V_s of the dried, shrunken cylinder sample was estimated rather roughly by measuring its mean height and diameter. In general, the form of the dried cylinder samples deviates strongly from an ideal cylinder. Most commonly, the dried cylinder surface becomes convex.

¹ Ludwig, W. J., Krashennnikov, V. A., et al., *Init. Repts. DSDP, 71*: Washington (U.S. Govt. Printing Office).

It was observed in a few stereoscan pictures that the porosity was not reduced homogeneously throughout the cylinder: high porosities are preserved at the outer margins, although strong shrinkage occurs in the center of the samples. The marginal pores are filled with salt. Thus the amount of local shrinkage seems to depend mainly on the length of time during which capillary forces are acting on the particles and on transport and deposition of the residual salts, which may cement the pores. Nevertheless, the shrinkage values may give some hints about the composition and diagenetic state of the sediments. For a detailed discussion of this property see Einsele (1982).

Vane Shear Strength and Penetration

Mechanical strength was measured with a Wykeham Farrance Laboratory Vane Apparatus (Boyce, 1977) and also with the needle penetrometer. The additional measurements by the needle penetrometer were made because the vane shear test may not be able to measure undrained shear strength in sediments with high diatom content, which tend to drain very quickly. For the penetration test, the needle was dropped from 1 cm above the sediment, parallel to the bedding. The vane shear test was done as recommended by Boyce (1977), with the vanes inserted parallel to the bedding planes. Remolded shear strength was not measured, because of time constraints. However, at Sites 513 and 514 an attempt was made to measure the whole stress-strain relationship within 90° of strain, in order to relate the topological stress-strain pattern to sedimentology.

Sonic Velocity

Where the sediment was not lithified, all measurements of compressional sonic velocity were taken through the core liner of the working half of the core, using the shipboard Hamilton Frame Velocimeter (Boyce, 1976a). A correction factor for the liner was used. Although some problems are associated with this measuring method (varying thickness of the liner, unknown thickness of coring mud), several tests demonstrated that it gave much better results than the cylinder or the chunk technique. Internal fracturing that occurs in sampling with the cylinder or in cutting a chunk may cause marked lowering of the sonic velocity, although bulk density measurements are affected little or not at all. Sonic velocity was measured repeatedly through the semistandard samples of Lucite, aluminum, and brass. Within the range of sonic velocity recorded in the sediments, no correction factor was necessary.

PHYSICAL PROPERTIES AND LITHOLOGICAL COMPOSITION VERSUS DEPTH

Depth itself only indirectly affects physical properties; here it serves as an independent scale to relate different trend curves for which the values have not been measured on identical samples. Figures 1-4 show the trend curves for lithological composition and for several physical properties of the sediments at Sites 511-514. Especially for lithological composition, these are generalized trends, since they were constructed from the mean values for each core; for the scattering of the original data see the site chapters (this volume) and Figures 5 to 8.

Porosity, bulk density, and water content are affected by compaction, cementation, and lithological composition of the sediments. Holes 512-514 and the upper 180 meters in Hole 511 show that down to more than 200 meters, the mass physical properties are much more affected by sediment composition than by compaction. In particular, sediments which contain 40% or more diatoms show extremely high porosities and therefore low bulk densities. In diatom oozes down to 180 meters, the porosity stays between 80 and 85% and a compaction gradient is not recognizable, although compositional fluctuations are clearly repeated by the porosity, water content, and bulk density curves. The main source of porosity in diatomaceous sediments is intraskeletal space, which is preserved to rather great burial depth by the high strength of diatom shells (Calvert, 1974; Einsele, in press). In contrast, clays show typical compaction curves (Hole 511 below 180 m; Hole 514 below 50 m), although compositional changes are quite recognizable. Below 200 meters depth, an increasing nannofossil content causes a change: pore volume is reduced not by

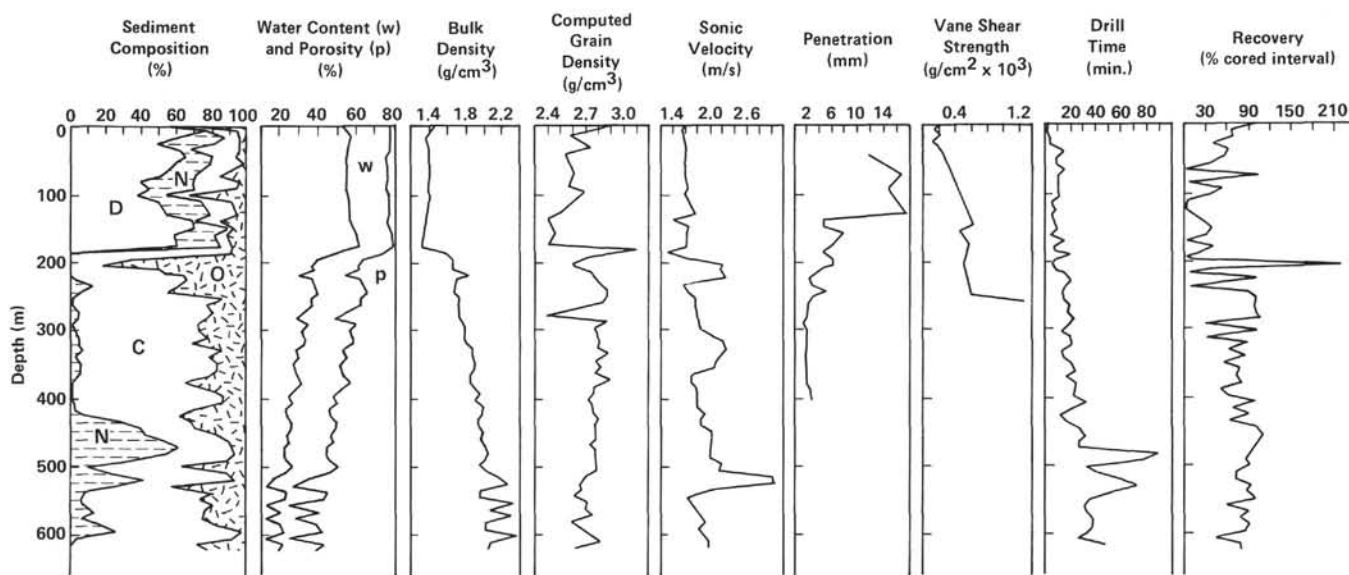


Figure 1. Depth logs of sediment composition, physical properties, and coring summary for Site 511. Data are mean values for cores. (D = diatoms, N = nannofossils, C = clay content, O = other components.)

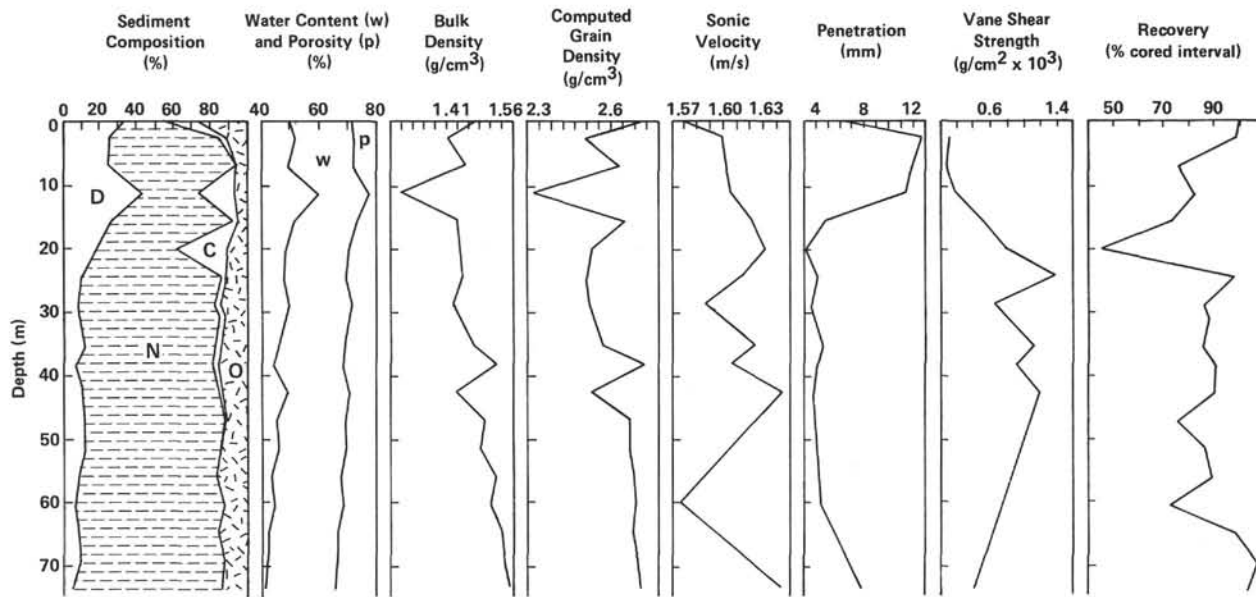


Figure 2. Depth logs of sediment composition, physical properties, and coring summary for Site 512. Data are mean values for cores. (D = diatoms, N = nanofossils, C = clay content, O = other components.)

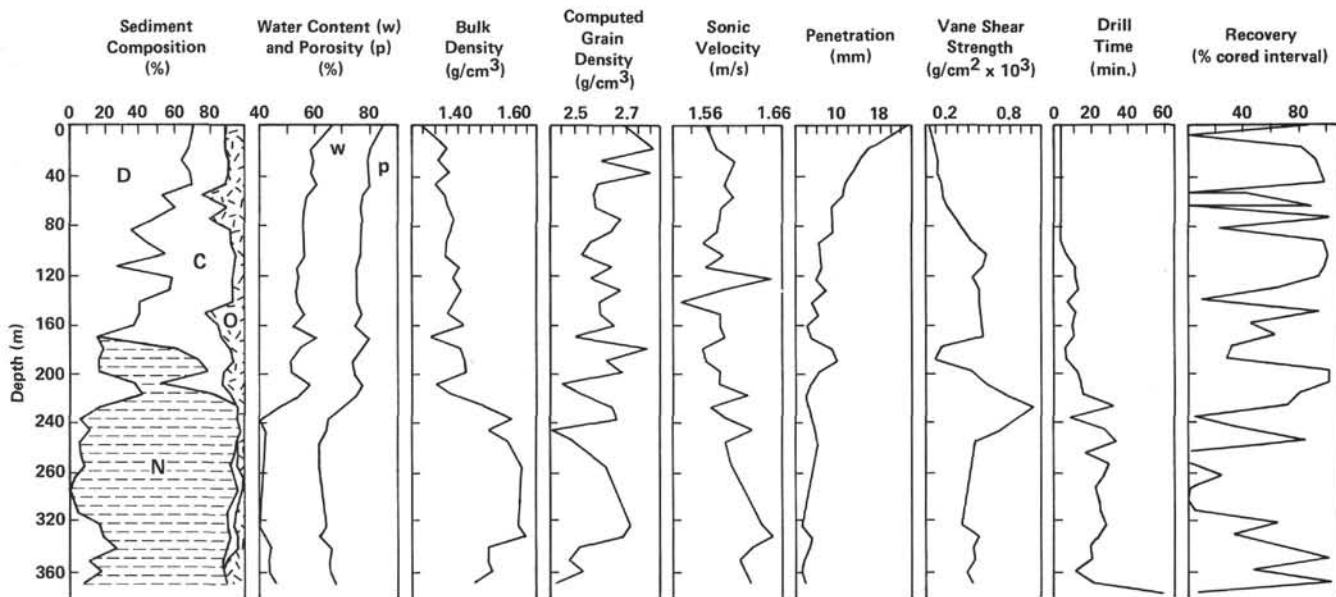


Figure 3. Depth logs of sediment composition, physical properties, and coring summary for Site 513. Data are mean values for cores. (D = diatoms, N = nanofossils, C = clay content, O = other components.)

compaction but by cementation (Hole 511). The Site 512 data, however, indicate a normal compaction curve for nanofossil oozes down to 80 meters. These results seem to agree with Schlanger and Douglas (1974), who, for nanofossil oozes, record an early compactional dewatering stage near 200 meters depth.

The *vane shear strength* increases rather slowly with diatomaceous oozes and muds; the curve is steeper for clays (Hole 514). Rather high shear strength values are reached in nanofossil oozes at shallow depths (Site 512). The reduction of vane shear strength in Site 512

below 40 meters is due to core disturbance, which may also have caused the relatively low shear strength values in the lower section at Site 513, where *drilling time* may be a better indicator of relative shear strength than the laboratory values. The penetration values, in principle, inversely repeat the shear strength data, although they are less sensitive to core disturbance because a much smaller "undisturbed sample" can be used for this test.

Figures 5-8 give a somewhat different type of trend analysis. The trend curves (thick lines) have been estimated by an unweighted moving mean whereby the area

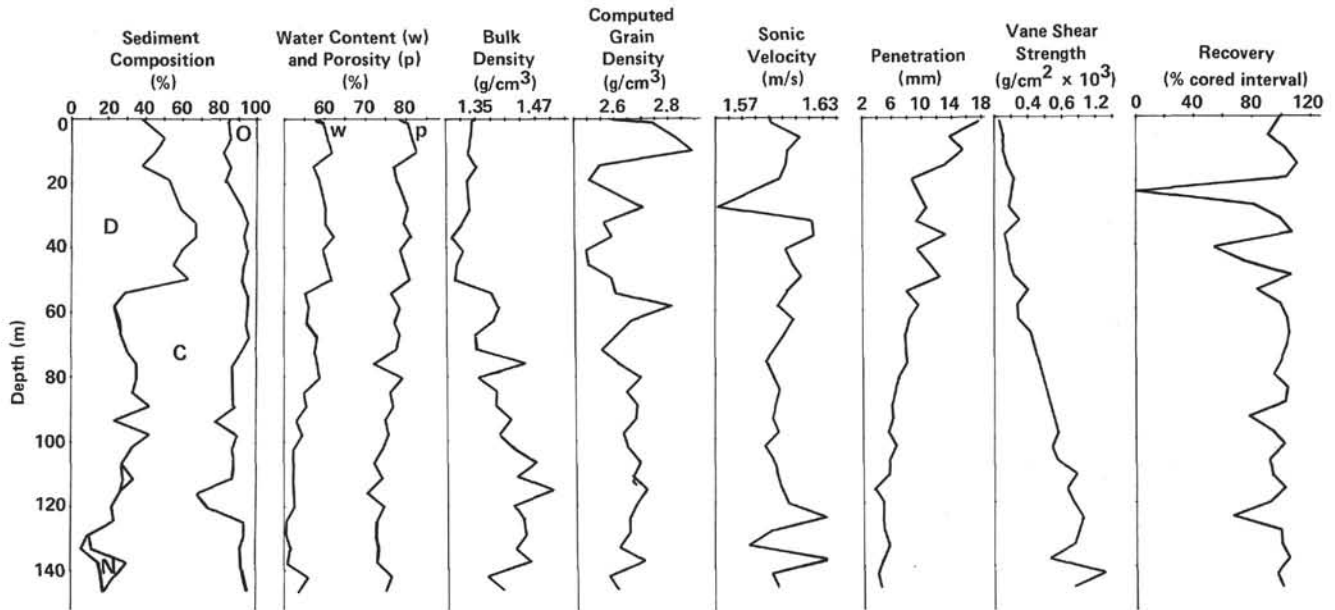


Figure 4. Depth logs of sediment composition, physical properties, and coring summary for Site 514. Data are mean values for cores. (D = diatoms, N = nanofossils, C = clay content, O = other components.)

of influence has been set approximately according to core length: 5 meters at Sites 512 and 514, 10 meters at Sites 511 and 513. Gaps within the trend curve are due to missing samples, that is, little or no recovery. Besides porosity and clay content, shrinkage and CaCO_3 values (from carbonate bomb data) are represented. The maximum peaks of the trend curves are sometimes slightly dislocated, especially near erratic shifts in the original data; this type of dislocation is a special property of the unweighted moving average and has to be taken into account when the curves are compared. The trend curves again indicate the dependence of porosity upon diatom content (high values) and nanofossil or CaCO_3 content (low values). The shrinkage data are influenced mainly by the CaCO_3 content. Thus at Site 513 the shrinkage values drop rapidly at 160 meters depth. But the data do not allow one to determine whether shrinkage is affected mainly by porosity or CaCO_3 content, because porosity also drops as CaCO_3 content increases (Sites 512, 513).

In contrast to the other physical properties, sonic velocity shows practically no depth-dependence, and most fluctuations of this measurement cannot be related to other parameters. Only at Site 511 is there a clear increase of sonic velocity with depth. Three peaks are superimposed on the trend. Within the uppermost 180 meters where the diatom content is high, the sonic velocity stays constant at values between 1.5 and 1.6 km/s. At 200 meters, high sonic velocities of 2.0 km/s can be related to high percentages of unspecified carbonates (10–70%) and high zeolite contents (30%); at 500 meters, dense, cemented layers of nanofossil chalk reach sonic velocities of 3.0 km/s. The cause of the third peak at approximately 350 meters is less obvious. It occurs in a series of well-stratified to laminated clays which contain layers of calcareous fossils (*Inoceramus*)

in the lower part. The bedding may have caused somewhat higher velocities, which were measured parallel to the laminae (Boyce, 1976b; Nacci et al., 1974).

EFFECT OF SEDIMENTOLOGICAL COMPOSITION UPON INTERRELATIONSHIPS AMONG PHYSICAL PROPERTIES

Bulk Density

Formally, the interrelationships of mass physical properties are fully described by the following set of linear equations:

$$\rho_b = \sum_{i=1}^n V_i \rho_i \quad (1)$$

$$\sum_{i=1}^n V_i = 1$$

where ρ_b = wet-bulk density,
 ρ_i = component density, and
 V_i = fractional volume.

The equations have the character of a continuity equation. The system is defined by the $2n$ parameters V_i and ρ_i , or by ρ_b and $n-1$ products of $V_i \rho_i$. By simple transformations, all commonly used measurements for mass physical properties can be developed from the equations. For example, wet content measurements simply require a division by ρ_b :

$$w_i = \frac{V_i \rho_i}{\rho_b}, \quad \sum_{i=1}^n \frac{V_i \rho_i}{\rho_b} = 1 \quad (2)$$

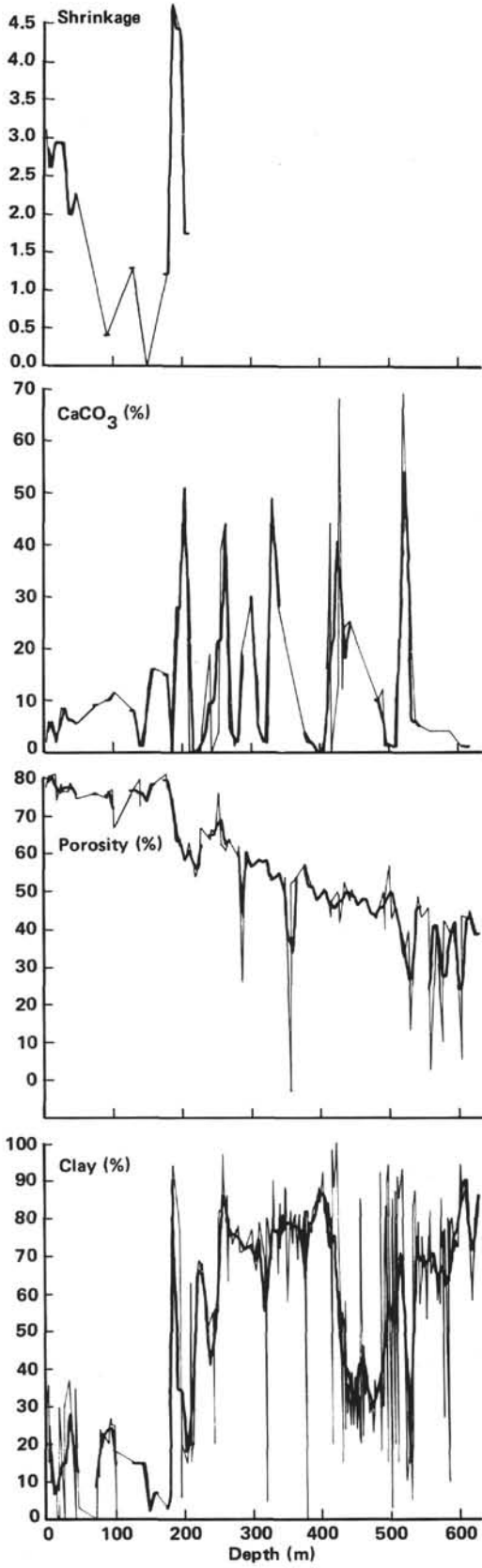


Figure 5. Depth logs for shrinkage, CaCO₃ content, porosity, and clay content from Site 511. Thin lines are original data; thick lines represent a trend estimated by an unweighted moving average.

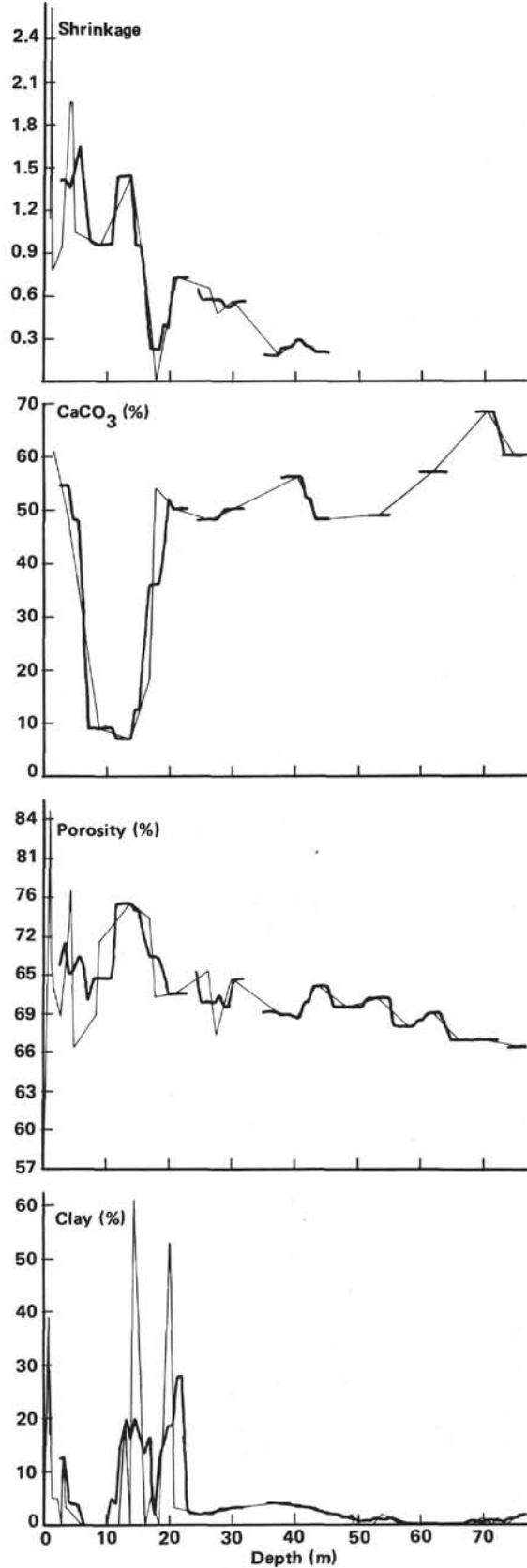


Figure 6. Depth logs for shrinkage, CaCO₃ content, porosity, and clay content from Site 512. Thin lines are original data; thick lines represent a trend estimated by an unweighted moving average.

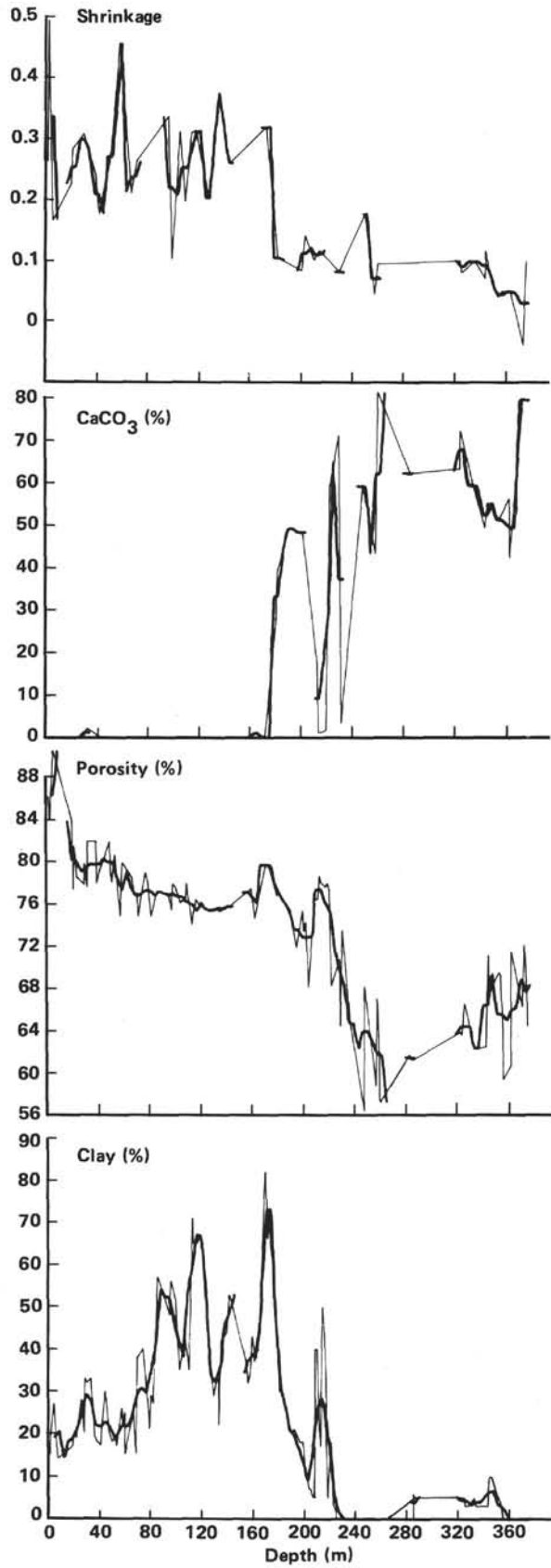


Figure 7. Depth logs for shrinkage, CaCO₃ content, porosity, and clay content from Site 513. Thin lines are original data; thick lines represent a trend estimated by an unweighted moving average.

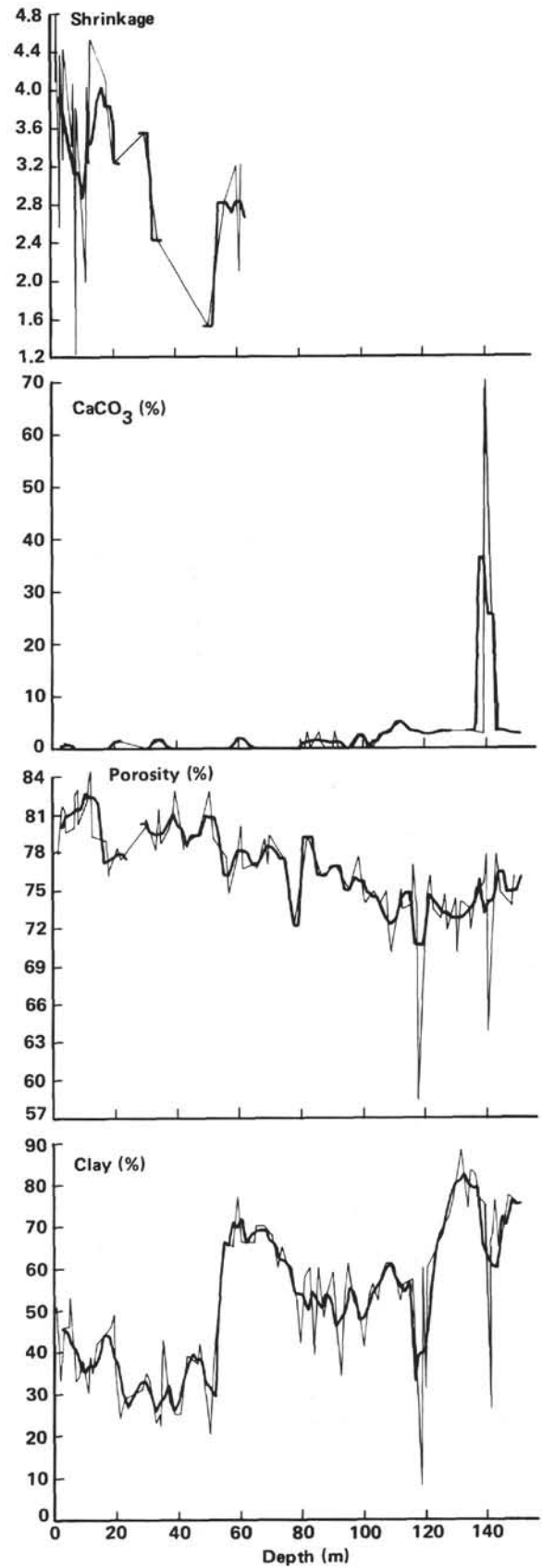


Figure 8. Depth logs for shrinkage, CaCO₃ content, porosity, and clay content from Site 514. Thin lines are original data; thick lines represent a trend estimated by an unweighted moving average.

Under the assumption that the sediment is at its natural pore-water content and that it does not contain gas, the first set of equations is reduced to the well-known form

$$\rho_b = \phi \rho_w + (1 - \phi) \rho_s; \sigma \leq \phi \leq 1, \quad (3)$$

where ρ_s = density of solids, and ϕ = fractional porosity.

Following Richards et al. (1974), the water density ρ_w is set to 1 in this study, because the data for a real salt correction are not available and an estimated mean correction (Boyce, 1976a) causes only slight differences.

Under the assumption of known interstitial water density, the functional relationship between bulk density and porosity has to pass through the point ($\phi = 1$, $\rho_b = 1$). The whole linear relationship can then be estimated either by a second point on the line—that is, the mean grain density—or by a least square approximation of the inclination. For a regression analysis, equation 3 can be rewritten as

$$\rho_b = \rho_s + (\rho_w - \rho_s) \phi, \quad (4)$$

or, in terms of a regression line, as

$$\rho_b = a + b \phi. \quad (4a)$$

From equations 4 and 4a we find that a standard regression technique using least squares allows one to estimate mean grain density and mean interstitial water density from the bulk density–porosity scattergram:

$$\rho_s = a; \rho_w = b + a.$$

A regression analysis using equation 4 was carried out for Sites 511–514; the results are summarized in Figure 9 and Table 1. For these regressions, all the shipboard data have been used and relationships of bulk density versus porosity and of porosity versus bulk density have been determined. The square of the Pearsonian correlation coefficient (r^2) is given as a measurement of the quality of approximation, but it should not be interpreted as a statistical measurement, because in this context “regression” simply means a least square approximation and not at all a likelihood approximation. It cannot be assumed that the residual distribution off the regression line follows a Gaussian distribution pattern, but it may nonetheless be due to systematic density changes within the sites. Table 1 indicates a rather high uncertainty for the estimated densities that can in part be related to variations that exist in sediment composition.

The influence of the sediment composition could, in principle, be analyzed by multiple regression techniques using the composition data (derived from the somewhat imprecise smear slide data). The Leg 71 data do not allow this strategy, because the composition data were not taken from the physical property samples and because the porosity and bulk density ranges vary for different lithological compositions. Therefore, mean com-

positional values derived from smear slide analysis have been used to study the influence of composition on the physical properties of the cores. This strategy, of course, will reduce resolution because the composition data are qualitative in nature and are average over cores. Nevertheless, systematic trends are recognizable.

The data have been subdivided into three groups of samples, which consist of more than 50% clay, diatoms, or nanofossils, respectively. Figure 10 and Table 2 summarize the results for regressions through the point ($\phi = 1$, $\rho_b = 1$). Figure 11 and Table 3 present results for the standard regression method, which gives a measurement for the linear relationship by the associated correlation coefficient.

As can be seen from the scattergrams (Figs. 10, 11), the range of porosity for the diatomaceous oozes is very small; therefore, the results of the regression equations for these data have to be treated with care. Nevertheless, the grain densities estimated from the regression line forced through the point ($\rho_b = 1$, $\phi = 1$) yield reasonable values for clay (2.7 g/cm³) and diatomaceous oozes (2.58 g/cm³). The value for the nanofossil oozes (2.63 g/cm³) is somewhat small in comparison with the density of pure calcite. The general regression model gives a grain density around 2.8 g/cm³ for the nanofossil oozes, a reasonable result for chalk. Differences between the two solutions are caused mainly by a few data points at which porosities are less than 50%. Although there may be too few data, the result may be compared with those of Schlanger and Douglas (1974), who found that the change from nanofossil ooze to chalk does not seem to be caused by a change in porosity and that it occurs by cementation, within a thick interval of almost constant densities. Furthermore, they observed that the change from compaction to cementation in nanofossil oozes occurs within a porosity range of 65–40%, a finding which would agree with the data analyzed here. The general regression analysis also gives an estimation of the grain density for diatomaceous oozes (2.34 g/cm³) which is close to the pure end-member (opal, 2.2 g/cm³). The uncertainty, however, is reasonably high, because the inverse regression line indicates density values of 2.96 g/cm³. The estimated grain density for the clay data in both regression models is about 2.71 g/cm³. Some of the low-porosity clay data reflect high carbonate contents, either from unspecified carbonates or nanofossils, and most of the data above the regression line in Figure 11 (indicated by Z) show diagenetic alteration through the formation of carbonates and zeoliths.

The solution for the estimated fluid density from the general regression equation gives values of less than 1 for clay and nanofossil oozes. Because the porosity values have not been corrected for salt content, we have to determine if the low fluid density values are artificial. For $\rho_b = 1$ we find, from the regression lines for the clay, $\phi = 0.99$, and from those for the nanofossil oozes, $\phi = 0.96$. Following Boyce (1976a), the conversion from uncorrected to corrected porosity is given by $\phi_{\text{corr}} = 1.0115 \phi_{\text{uncorr}}$; 35‰ salt. The inverse relationship also holds: $\phi_{\text{uncorr}} = 0.9886 \phi_{\text{corr}}$. Thus, for the uncorrected porosity we should estimate a value of 0.99

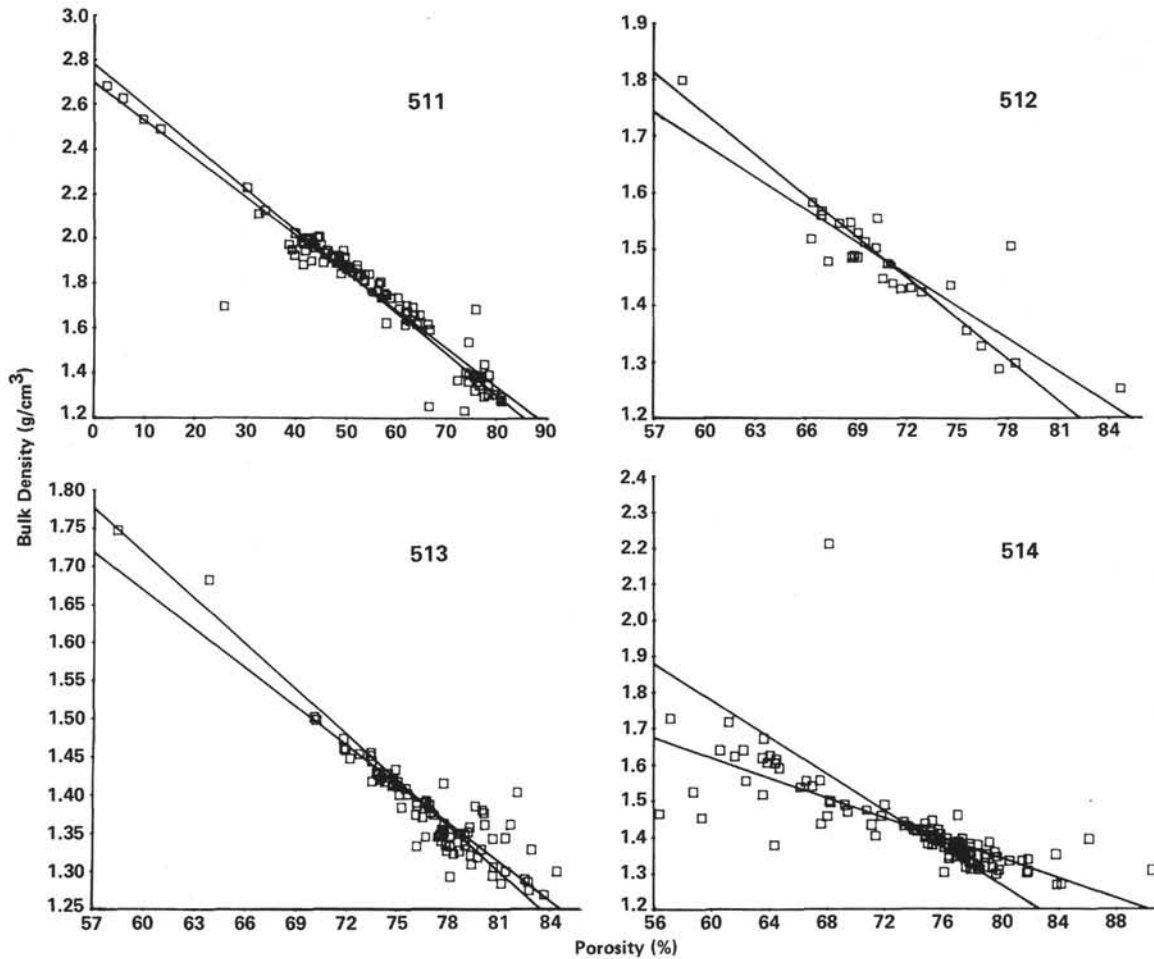


Figure 9. Relationship between bulk density and porosity for Sites 511 to 514, from original data. For regression equations, see Table 1.

Table 1. Relationship between bulk density (ρ_b) and porosity (ϕ), by site.^a

Site	Equation	Estimated Grain Density	Estimated Fluid Density	N	r ²
511	$\rho_b = -169\phi + 2.7$	2.7	1.1	103	0.92
	$\phi = -0.54\rho_b + 1.51$	2.8	0.94		
512	$\rho_b = -1.92\phi + 2.84$	2.84	0.92	28	0.79
	$\phi = -0.41\rho_b + 1.32$	3.22	0.78		
513	$\rho_b = -1.38\phi + 2.45$	2.45	1.07	104	0.54
	$\phi = -0.39\rho_b + 1.3$	3.33	0.77		
514	$\rho_b = -1.7\phi + 2.69$	2.69	0.99	85	0.85
	$\phi = -0.50\rho_b + 1.47$	2.94	0.94		

^a Estimated from original data.

for a bulk density of 1.0. This fits the clay data very well, but a difference still exists for the nannofossil oozes. In fact, the range of values for porosity and bulk density is very small with respect to data scattering.

Shrinkage

A first approximation for the equilibrium curve of compaction can be given by the equation

$$\frac{d\phi}{dp} = -C\phi, \tag{5}$$

where ϕ = porosity, and p = pressure; this simply states that an increase of effective pressure causes a decrease in porosity that is proportional to the momentary pore volume. As the pore volume goes to zero, compaction goes to zero. The constant c can be interpreted as a coefficient of volume change (Terzaghi, 1943), which is specific for particular materials. Integrating (5), we get the model

$$\phi = \phi_0 e^{-cp}. \tag{5a}$$

Shrinkage is caused by capillary tension, and the shrinkage limits depend on the equilibrium between capillary tension and resistance to compression (Sowers, 1979). Internal tension acts like an external pressure (Einsele, 1982). Therefore, the equilibrium states of shrinkage and the development of shrinkage limits are described by the compaction model, equation 5a or by

$$sh = sh_0 e^{-C_s p}, \tag{6}$$

which has been statistically proven to linearize the data. From the models (5a) and (6), shrinkage can be related to porosity by the equation

$$sh = a\phi^{-b}, \tag{7}$$

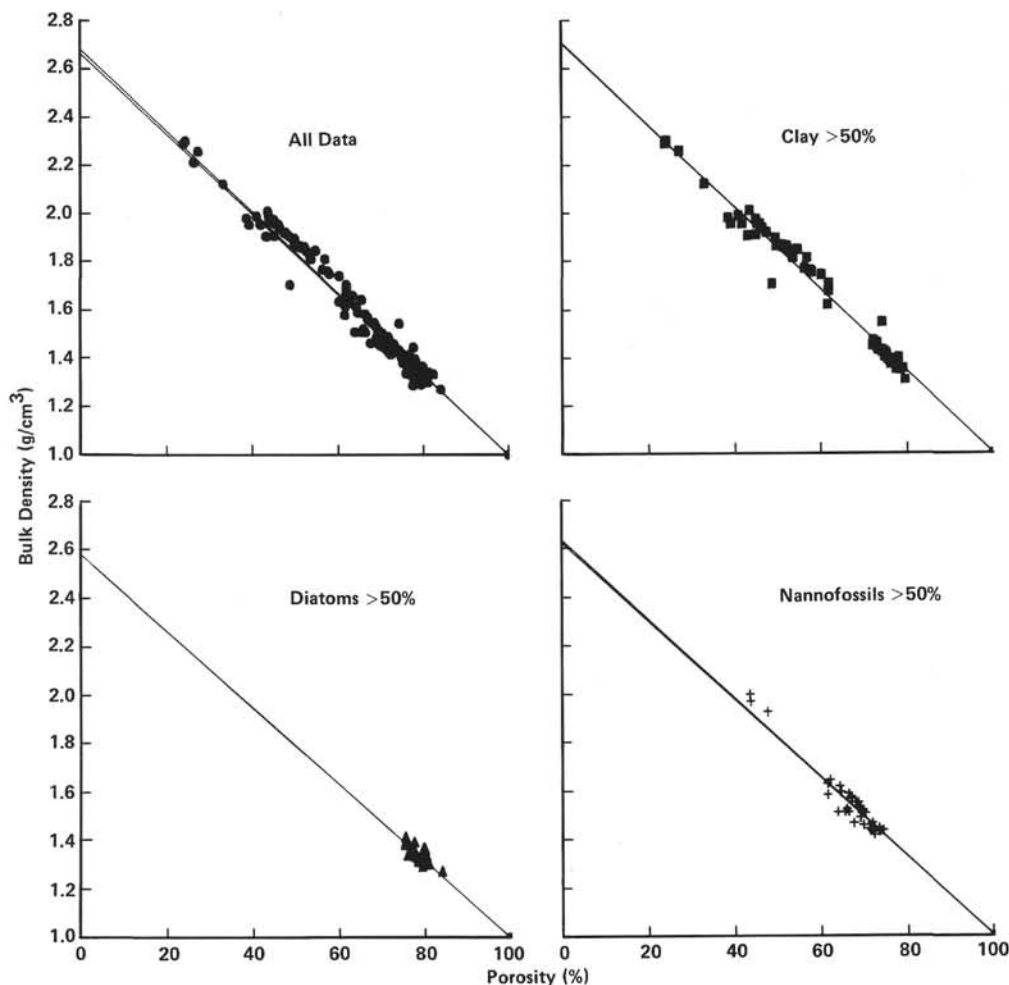


Figure 10. Linear relationship between bulk density and porosity, for mean values of cores: all data, and sediments grouped by primary components. The regression lines pass through the point ($\phi = 1$; $\rho_s = 1$); see Table 2.

Table 2. Relationship between bulk density (ρ_b) and porosity (ϕ); main components passing through ($\phi = 1$, $\rho_s = 1$).^a

Condition	Equation	Estimated Grain Density	Fluid Density	N
Data for all sites	$\rho_b = -1.66\phi + 2.66$ $\phi = -0.6\rho_b + 1.6$	2.66 2.67	1	145
Sediment grouped by primary components				
Clay content >50%	$\rho_b = -1.71\phi + 2.71$ $\phi = -0.59\rho_b + 1.59$	2.71 2.69	1	59
Diatom content >50%	$\rho_b = -1.58\phi + 2.58$ $\phi = -0.63\rho_b + 1.63$	2.58 2.59	1	25
Nannofossil content >50%	$\rho_b = -1.63\phi + 2.63$ $\phi = -0.61\rho_b + 1.61$	2.63 2.64	1	31

^a Data are mean values for the cores.

which may be linearized as

$${}^e\log(sh) = {}^e\log a - b{}^e\log \phi. \quad (7a)$$

The shrinkage-porosity relationships observed for the different sites are summarized in Figure 12 and Table 4. For Sites 512 and 513 the predicted model fits the data sufficiently if additional variation caused by

the sedimentological composition is taken into account. For Site 514, in contrast, the relationship is reversed: shrinkage increases with decreasing porosity. The depth distribution of shrinkage and porosity (Fig. 8) shows that the variation of porosity at Site 514 is not caused by compaction but by fluctuations of the clay-diatom content. The Site 514 data, therefore, indicate a strong dependence of the shrinkage values on the sedimentological composition. As can be expected (Einsele, in press), shrinkage increases with increasing clay content. Because porosity is reduced with increasing clay content in diatomaceous oozes and muds, an inverse relationship with porosity results if compaction can be ignored. The depth relationships for Site 513 indicate further a strong reduction in the shrinkage limits with increasing CaCO_3 content, but there are not enough data for a further analysis.

For Site 511, the limited amount of data does not allow an analysis.

Vane Shear Strength and Penetration

Vane shear and penetration data were used to measure the mechanical strength of sediments. Although the vane

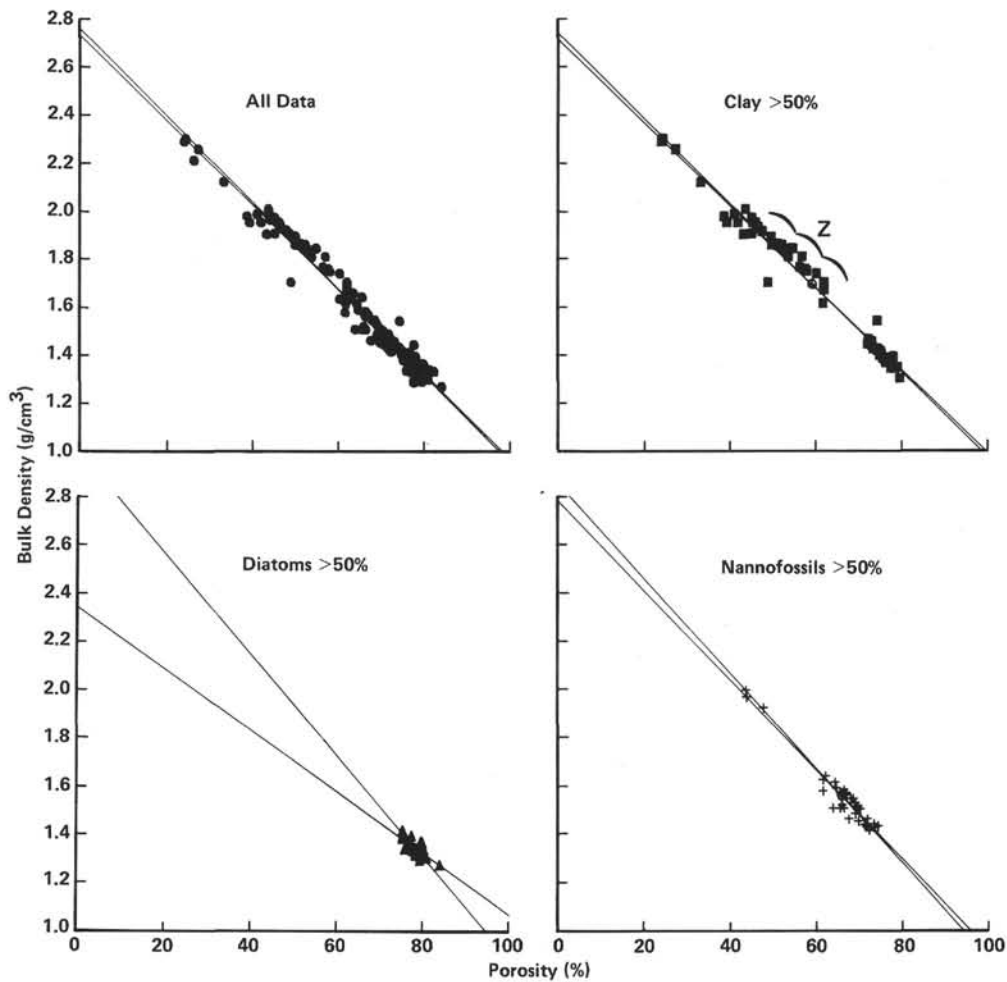


Figure 11. Linear regression between bulk density and porosity, for mean values of cores: all data, and sediments grouped by primary components. For regression equations, see Table 3.

Table 3. Relationship between bulk density (ρ_b) and porosity (ϕ) for sediments grouped by primary components.^a

Condition	Equation	Estimated Grain Density	Estimated Fluid Density	N	r ²
Data for all sites	$\rho_b = -1.76 \phi + 2.73$ $\phi = -0.555 \rho_b + 1.53$	2.73 2.78	0.97 0.96	145	0.976
Sediment group					
Clay content >50%	$\rho_b = -1.72 \phi + 2.71$ $\phi = -0.57 \rho_b + 1.55$	2.71 2.72	0.99 0.96	59	0.975
Diatom content >50%	$\rho_b = -1.28 \phi + 2.34$ $\phi = -0.48 \rho_b + 1.42$	2.34 2.96	1.06 0.89	25	0.61
Nannofossil content >50%	$\rho_b = -1.86 \phi + 2.78$ $\phi = -0.51 \rho_b + 1.45$	2.78 2.84	0.92 0.88	31	0.945

^a Data are mean values for the cores.

shear data give a measurement of shear strength (g/cm^2) under the special conditions of the cylindrical shear surface and the draining conditions (see Boyce, 1976b), the penetration values are only relative measurements. In general, a real calibration of penetration with vane shear measurements is impossible (Bennett and Keller, 1973). Both measurements depend on cohesion, friction, and dilatancy or compressibility, but it is not clear how these different factors will affect the two measurements. A statistical analysis for the main components of

the sediments showed that, in the context of several simple models, the relationship between vane shear strength and penetration can be described best by

$$\frac{d(\text{vane})}{d(\text{pen})} = \frac{C}{(\text{pen})}, \quad (8)$$

which leads to a linear relationship of the form

$$\log(\text{vane}) = a(\text{pen}) + b. \quad (8a)$$

The analysis of the main lithological components at the Leg 71 sites, using this model, is summarized in Figure 13 and Table 5. The relationship between vane shear strength and penetration depth is not independent of the lithological composition. There are slight differences between the measurements for the clays and nannofossil oozes which, if they reflect real difference in the sediments, may be related to compressibility and cohesion (lower penetration values in nannofossil oozes, higher shear strength in clays for the boundary values, $\log(\text{vane}) = 0$, and penetration = 0). Clearly diatomaceous oozes behave differently from other lithological

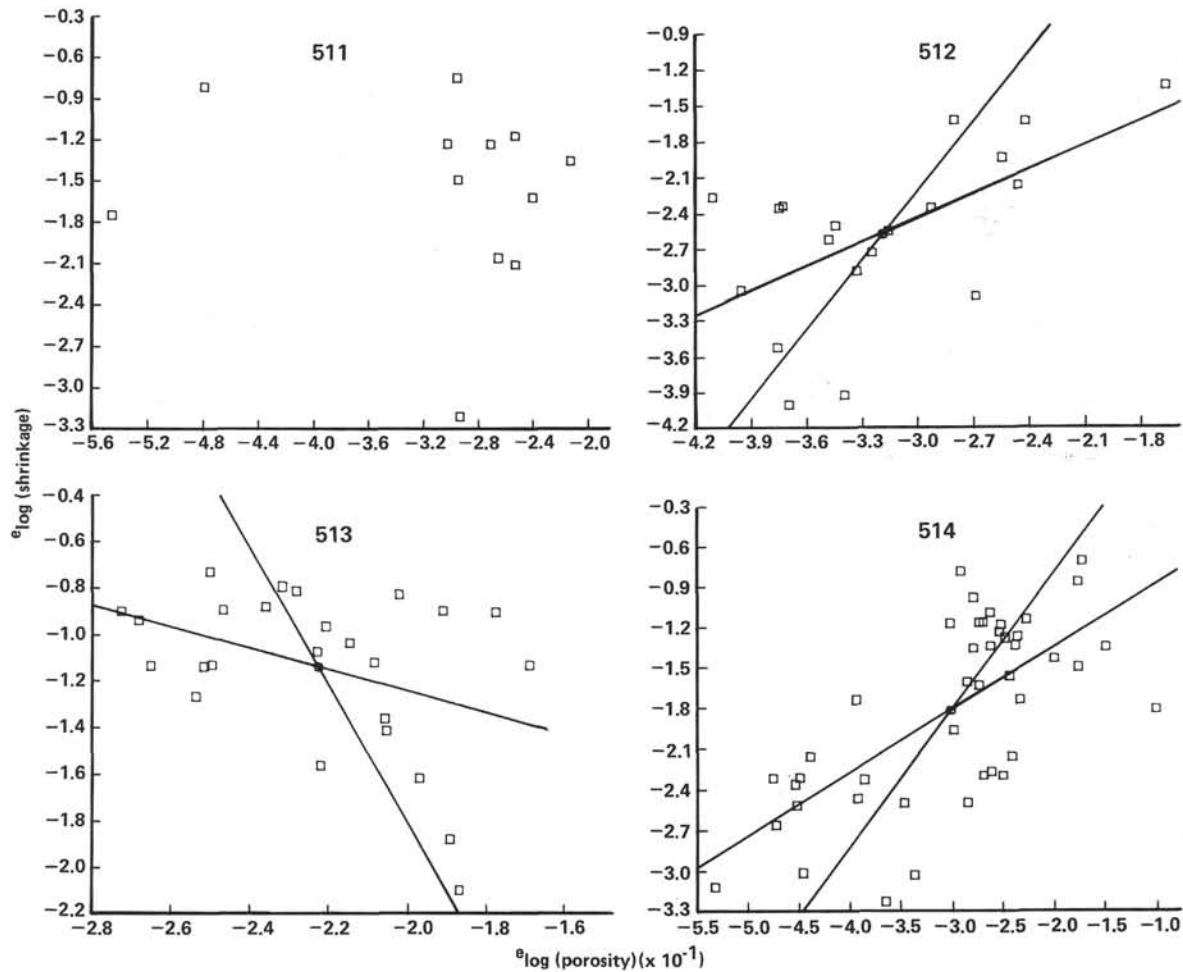


Figure 12. Relationship between $e \log(\text{shrinkage})$ and $e \log(\text{porosity})$ estimated from the original data for Sites 511–514. For regression equations, see Table 4.

Table 4. Relationship between shrinkage (sh) and porosity (ϕ).

Site	Regression Equation	Model	N	r^2
511	$e \log(sh) = -0.87 e \log \phi - 1.83$ $e \log \phi = -0.02 e \log(sh) - 0.39$	$sh = 0.16 \phi^{-0.87}$ $\phi = 0.72 sh^{-0.02}$	12	0.017
512	$e \log(sh) = 6.83 e \log \phi - 0.40$ $e \log \phi = 0.05 e \log(sh) - 0.19$	$sh = 0.67 \phi^{6.83}$ $\phi = 0.83 sh^{0.05}$	19	0.35
513	$e \log(sh) = 4.67 e \log \phi - 0.41$ $e \log \phi = 0.1 e \log(sh) - 0.12$	$sh = 0.66 \phi^{4.67}$ $\phi = 0.89 sh^{0.1}$	44	0.46
514	$e \log(sh) = -4.66 e \log \phi - 2.18$ $e \log \phi = -0.03 e \log(sh) - 0.26$	$sh = 0.11 \phi^{-4.66}$ $\phi = 0.77 sh^{-0.03}$	25	0.16

types, where high penetration and low vane shear values indicate that cohesion is lowered and dilatancy is increased with respect to the other types.

As with all physical properties, vane shear strength and penetration depend on porosity: friction will increase rapidly with decreasing porosity. Figures 14 and 15 and Tables 6 and 7 summarize the relationship of penetration and porosity for the different sites and for the main lithological types.

The model

$$\phi = a e \log(\text{pen}) + b \quad (9)$$

was used to relate penetration and porosity; it is sufficiently linear within the observed range of data. It turns out that there is no significant relation between the penetration values and the porosities in the Site 512 data (Fig. 14, Table 6), particularly for nannofossil oozes. The analysis by primary significant components (Fig. 15, Table 7) shows that only the clay data give a dependence between the variables; but only the clay data cover a sufficiently large range of porosities, whereas the diatom and nannofossil oozes are restricted to a much smaller range. The slopes for the regression equations of porosity versus $e \log(\text{pen})$ are identical for nannofossil and diatom oozes, and their relative porosity ranges are very similar. These similarities may indicate that the porosity–penetration relationships represent mainly compositional fluctuations in diatomaceous and nannofossil oozes, whereas the claystone values are dominated by compaction. This result is in agreement with the bulk density–porosity analysis. The penetration values indicate that there is little compaction of diatomaceous and even nannofossil oozes at less than 200 meters depth below seafloor.

During Site 513 operations, it was observed that two main shear types occurred in the sediments; they dif-

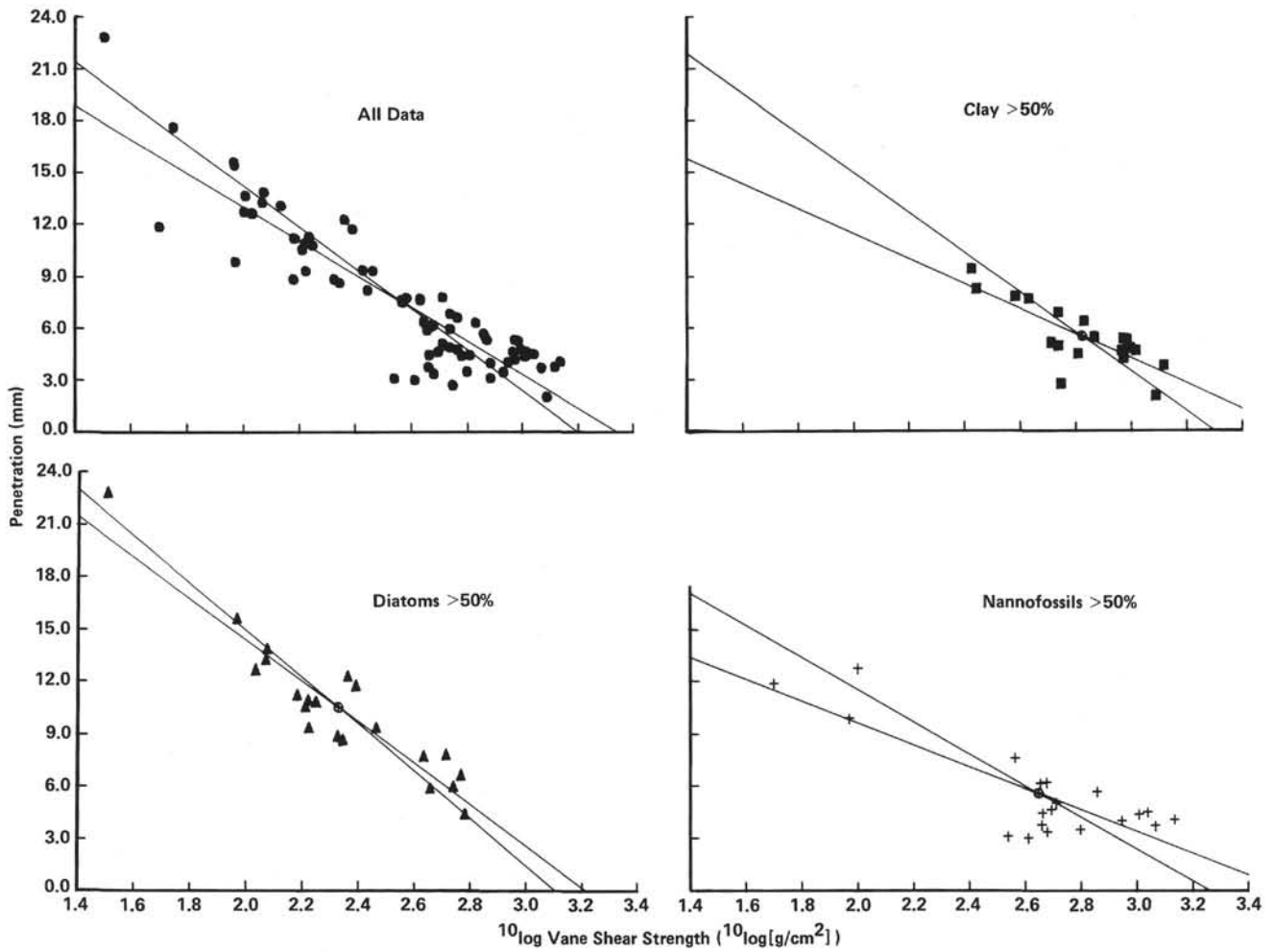


Figure 13. Relationship between penetration and vane shear strength, $10\log$ (vane shear strength), for mean values of cores: all data, and sediments grouped by primary components. For regression equations, see Table 6.

Table 5. Relationship between vane shear strength (*vane*) and penetration (*pen*) for sediments grouped by primary components.^a

Condition	Regression Equation	Model
Data for all sites	$10\log(vane) = -0.08(pen) + 3.2$ $pen = -9.74 \cdot 10\log(vane) + 32.5$	$(vane) = 1590.10^{-0.08 pen}$
Sediment group		
Clay content >50%	$10\log(vane) = -0.086(pen) + 3.29$ $pen = -7.29 \cdot 10\log(vane) + 26$	$(vane) = 1950.10^{-0.09 pen}$
Diatom content >50%	$10\log(vane) = -0.074(pen) + 3.1$ $pen = -11.81 \cdot 10\log(vane) + 38$	$(vane) = 1260.10^{-0.074 pen}$
Nannofossil content >50%	$10\log(vane) = -0.11(pen) + 3.26$ $pen = -6.24 \cdot 10\log(vane) + 22$	$(vane) = 1820.10^{-0.11 pen}$

^a Data are mean values for the cores.

ferred in the topology of the stress-strain curve and in the mode of failure.

During Site 514 operations, the stress-strain relationship was measured as accurately as possible throughout the whole range of the observable 90° of strain. Figure 16 summarizes the stress-strain diagrams for Site 514. The curves are grouped by their similarity and by depth. The resulting groups of “sensitive” and “insensitive” shear types do not show a relationship to the lithologic composition, but a relationship to the stratification of the sediments can be found. Well-stratified sediments

have a very distinct point of failure if vane shear strength is measured parallel to the lamination; homogeneous sediments are much more sensitive, especially in diatomaceous oozes and muds. In addition, the shear strength of stratified sediments seems to be somewhat higher than that of homogeneous sediments (Nacci et al., 1974). An idealized graph of the stress-strain relationship is given in Figure 17. The “insensitive” curves are drawn only to the point of failure; afterward, the strain pointer in general moved so fast that it was not possible to record enough data points for a reconstruction of the curve (dashed lines in Fig. 17). Figure 17 indicates that the topological behavior is not dependent on the maximum shear strength but that it is an independent property related to the macroscopic (and microscopic?) sediment structure of diatomaceous oozes and muds.

Sonic Velocity

The properties of sound have been extensively analyzed with respect to depth and bulk density because these relationships are important for practical seismic work (Hamilton, 1976b-d, 1978, 1979; Stoll, 1974; Taylor Smith, 1974). During Leg 71 operations, only compressional waves were measured. In contrast to shear

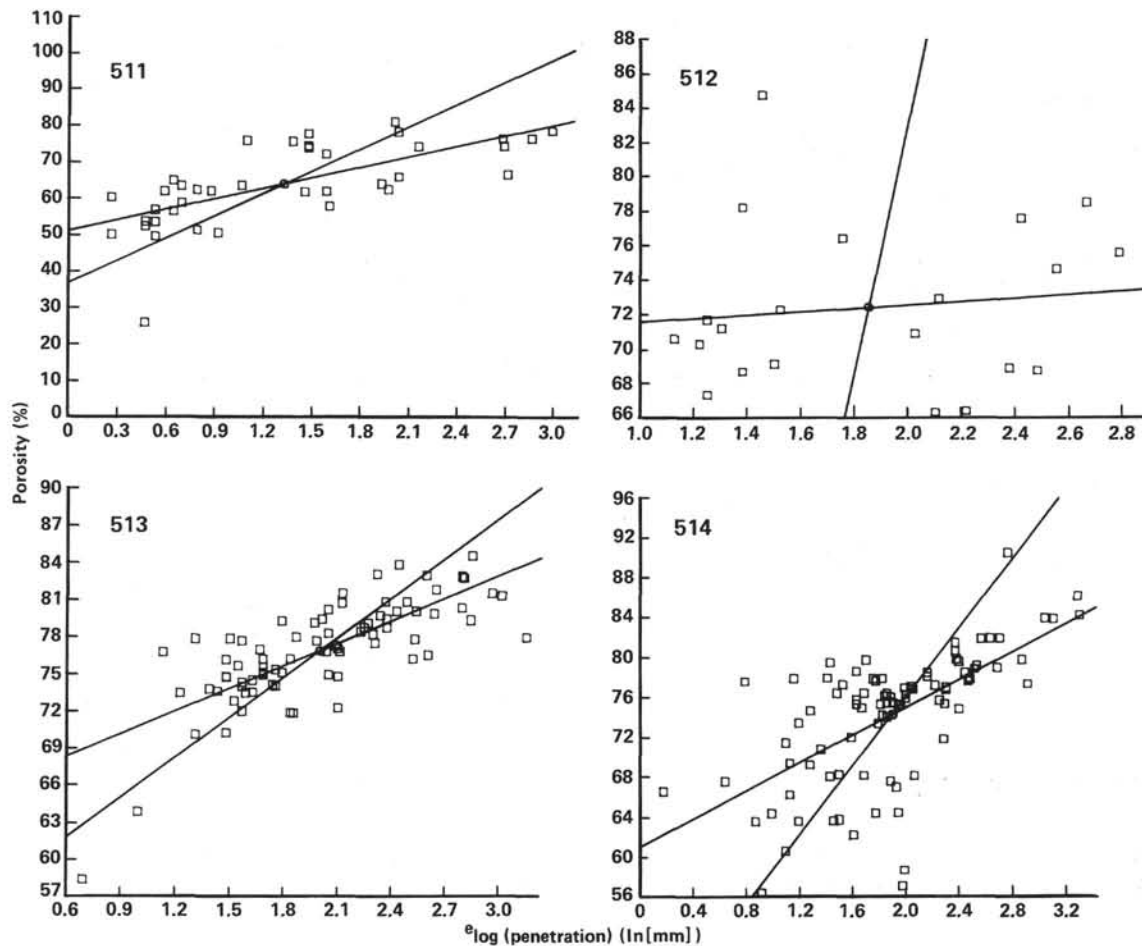


Figure 14. Relationship between porosity and $e^{\log(\text{penetration})}$, estimated from the original data, Sites 511 to 514. For regression equations, see Table 6.

Table 6. Relationship between penetration (pen) and porosity (ϕ), by site.^a

Site	Regression Equation	Model	N	r^2
511	$\phi = 0.098 e^{\log(\text{pen})} + 0.51$ $e^{\log(\text{pen})} = 4.89 \phi - 1.769$	$pen = 0.166 e^{4.89 \phi}$	38	0.479
512	$\phi = 0.01 e^{\log(\text{pen})} + 0.71$ $e^{\log(\text{pen})} = 1.40 \phi - 0.859$	$pen = 2.31 e^{1.4 \phi}$	21	0.014
513	$\phi = 0.07 e^{\log(\text{pen})} + 0.61$ $e^{\log(\text{pen})} = 5.761 \phi - 2.38$	$pen = 0.093 e^{5.76 \phi}$	89	0.40
514	$\phi = 0.06 e^{\log(\text{pen})} + 0.65$ $e^{\log(\text{pen})} = 9.34 \phi - 5.19$	$pen = 0.006 e^{9.38 \phi}$	79	0.57

^a Estimated from original data.

waves, these generally show little or no relationship to other mechanical parameters, such as shear strength (Nacci et al., 1974).

Sonic velocity versus depth for Site 511 seemed to indicate that the compressional sonic velocity depends much more on diagenetic and cementational processes than on compaction, although reduction of the pore volume by compression is also clearly a recognizable factor. In the literature most authors (Hamilton, 1978; Nacci et al., 1974) agree that porosity is one of the most important factors, more important than bulk density. Nacci et al. (1974) also emphasize that the number and

type of grain contacts are more important even than porosity.

To analyze the Leg 71 data a simple linear regression analysis of sonic velocity versus porosity was undertaken for the different sites (Fig. 18; Table 8) and again for the main components (Fig. 19, Table 9). The linear model fits the measured data sufficiently (in a statistical, not a physical sense) within the observed minimal and maximal bounds.

The data for Sites 511, 512, and 513 (Fig. 18, Table 8) indicate a statistical relationship between sonic velocity and porosity, but there is again little evidence for a dependence of velocity on porosity within the Site 514 data, which are derived mainly from diatomaceous sediments. The main-component analysis gives a very similar pattern. Throughout the observed porosity range, the diatomaceous oozes show very constant sonic velocities of about 1.6 km/s. The nannofossil oozes also fail to show a very clear relationship to porosity within the porosity range 75–60%. A somewhat more pronounced relationship is found within the clays. From a detailed analysis, however, we find that the higher velocity values at porosities less than 65% correspond to cores where increased contents of unspecified carbonate and zeolites indicate diagenetic alteration. The summary

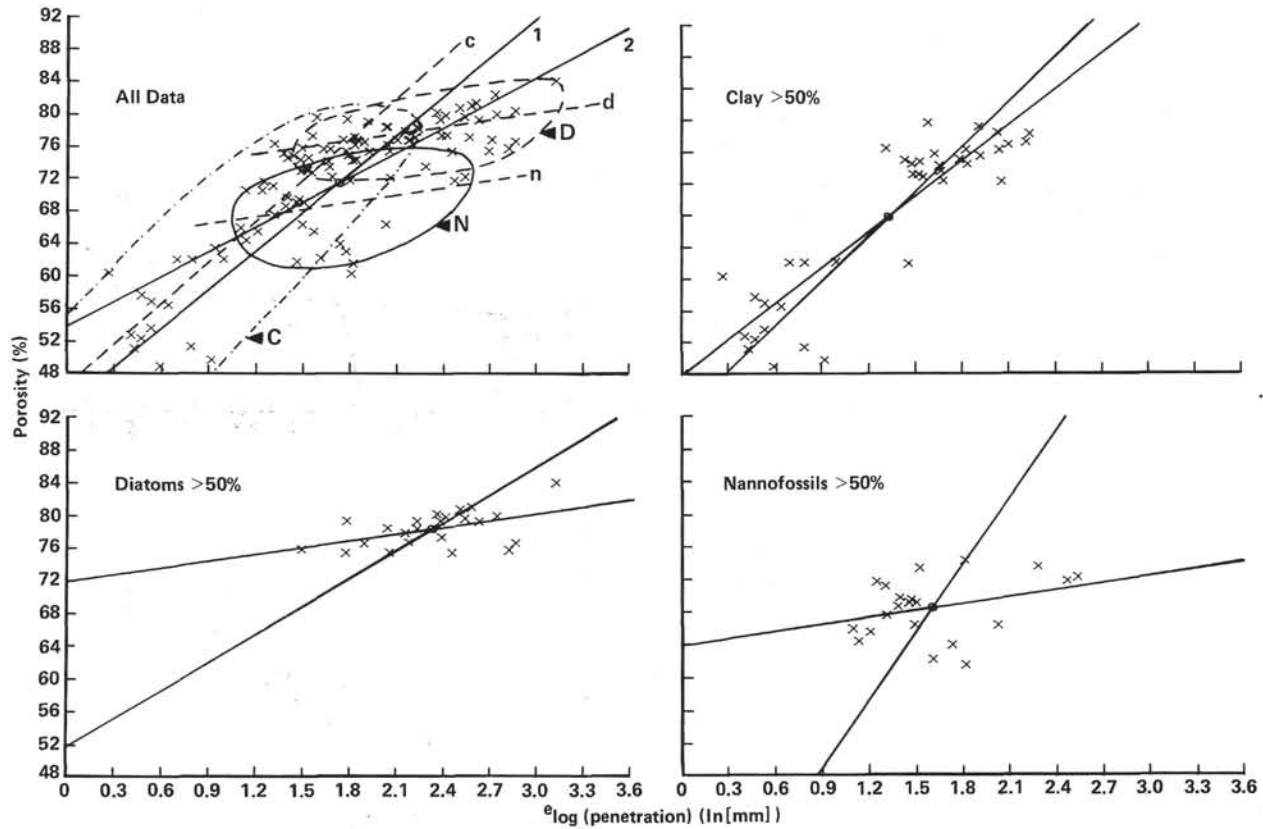


Figure 15. Relationship between porosity and $e \log(\text{penetration})$, for mean values of cores: all data, and sediments grouped by primary components. Upper left: N = nannofossil oozes; D = diatomaceous oozes; C = clay; (1,2) indicate the regression lines for all data.

Table 7. Relationship between penetration (pen) and porosity (ϕ); sediments grouped by primary components.^a

Condition	Regression Equation	Model	N	r ²
Data for all sites	$\phi = 0.10 e \log (pen) + 0.54$ $e \log (pen) = 6.31 \phi - 2.78$	$pen = 0.06e^{6.31 \phi}$	104	0.645
Sediment group				
Clay content > 50%	$\phi = 0.15 e \log (pen) + 0.48$ $e \log (pen) = 5.32 \phi - 2.27$	$pen = 0.10e^{5.32 \phi}$	38	0.797
Diatom content > 50%	$\phi = 0.03 e \log (pen) + 0.72$ $e \log (pen) = 8.68 \phi - 4.47$	$pen = 0.01e^{8.68 \phi}$	23	0.246
Nannofossil content > 50%	$\phi = 0.03 e \log (pen) + 0.64$ $e \log (pen) = 3.63 \phi - 0.87$	$pen = 0.42e^{3.63 \phi}$	21	0.106

^a Data are mean values for the cores.

graph for all data in Figure 19 gives an interpretation of the observed sonic velocity–porosity relationship. There is little change of the sonic velocity down to porosities of 60%, independent of the main component type. Then the clays with lower porosities show an increase in sonic velocity, to approximately 2 km/s at a porosity of 40%, which can be related to compaction. Besides compaction, diagenesis within clays and nannofossil oozes with porosities less than 60% increases sonic velocity rapidly. This may be related to cementation and fixation of the particles or at least to a reduction in plastic deformability. Thus, the “magic” porosity (45–60%) that Schlanger and Douglas (1974) found to be the range for a change from compaction to cementation in nannofossil oozes seems to hold for calcareous clays too.

There are several sophisticated formulas relating sonic velocity to porosity, such as those of Wood and of Nafe and Drake. One of the most interesting ones is the “time average formula” (Wyllie et al., 1958):

$$\frac{1}{V} = \frac{\phi}{V_f} + \frac{1 - \phi}{V_s}, \tag{10}$$

Besides its simplicity it has some interesting properties for use in statistical analyses. The time average formula simply states that the inverse velocity is given by the harmonic mean of the fluid velocity V_f and the velocity of the solid V_s (an extension for more than one component of solids should also be possible). As Hamilton (1978) pointed out, there are reasons to doubt that the formula will fit all types of porous media. Originally it was developed from a model of homogeneous layers. But if equation 10 is rewritten in a way similar to the bulk density–porosity relation in equation 4, then we get a linear model which allows one to estimate the sonic velocity V_f of the interstitial fluids and the velocity of solids V_s from the observed compressional velocities V and the porosity values:

$$\frac{1}{V} = \left(\frac{1}{V_f} - \frac{1}{V_s} \right) \phi + \frac{1}{V_s}. \tag{11}$$

A graphic and tabular representation of this model for primary components is given in Figure 20 and Table 10.

The pattern turns out to be somewhat curious. The V_s and V_f values for the diatomaceous oozes are identical (1.6 km/s, i.e., there is no dependence upon porosity). For the nannofossil oozes down to a porosity of 60%, the estimated velocity values are still very similar ($V_s = 1.79$, $V_f = 1.5$ km/s V water).

The difference in the velocity values increases if a single point with low porosity (48%) is taken into account ($V_s = 2.98$, $V_f = 1.39$). These values are identical with the clay data ($V_s = 2.98$, $V_f = 1.39$), which have a higher porosity range. These V_f values of approximately 1.4 km/s are within a reasonable range for the fluid velocities, if fluctuations of temperature and the uncorrected porosity values are taken into account. One wonders if the time average model could be used to analyze the types of grain contact that develop during compaction and diagenesis. The estimated velocities could be interpreted as reflecting the way that high-porosity diatomaceous oozes and similar nannofossil oozes behave—much more like a suspension than a system of two components ($V_f = V_s$). As grain contact increases through compaction and cementation, a two-component system develops and passes beyond into a final solid. A more detailed study of this model may be the subject of future work.

CONCLUSIONS

The possible number of interrelationships among physical properties is large, especially if different equivalent measurements, like porosity and void ratio, are used. Most interrelationships, however, are not independent and therefore give no additional information.

Physical properties can be understood as characteristic parameters not only for a given sample of rock, but for a dynamic system in which values change as the sediment structure develops during aging, compaction, and diagenesis. In that sense, physical properties are the momentary measurable output of a developing system. The system may be best described by the most simple relationships such as (1) the linear porosity–bulk density relation, (2) the time average equation as a model for the dependence of sonic velocity on porosity, or (3) simple exponential models. In contrast to complex polynomial approximations, these simple models allow one to interpret the parameters in terms of basic physical properties of the different phases of the sample. These esti-

mated values can then be tested against known boundary values and their physical and sedimentological meaning discussed.

The simplest form of such models—two-dimensional least square approximation of linearized relationships—was used here to analyze the development of physical properties with respect to compaction and sedimentological composition. The results indicate a separation of the Leg 71 data into two distinct groups, the Mesozoic sediments (mainly claystones) of Site 511 and the Tertiary and younger sediments from all sites. Only the Site 511 sequence shows a typical compaction curve and diagenetic alterations which affect the physical property data—porosity, bulk density, and sonic velocity. The Mesozoic data show that sonic velocity is much more affected by diagenetic, mainly cementational processes than by pure compaction. The diatomaceous and nannofossil oozes from the Tertiary and Quaternary sequences show very little compactional alteration. Nevertheless the mechanical properties, shear strength and penetration, clearly develop greater strength with depth. Especially in diatomaceous oozes, but also in nannofossil sediments, small decreases in porosity seem to increase grain to grain contact and cohesion rapidly. In contrast, the compactional sonic velocity values show very small changes; the observed variability can be related to compositional fluctuations of the sediment.

The behavior of sonic velocity and vane shear strength could be related to the development of the water cover of the particles. This influences cohesion and may preserve a “liquid” state for compressional sound waves until the particles are cemented during diagenesis. This aspect would agree with the shrinkage analyses. Shrinkage depends on the speed of drying, that is, the time tensional forces take to act, and as Einsele (in press) noted, the porosity of shrunken samples tends toward values similar to the “induration porosities” at which the material becomes firm. In sediments poor in diatoms these porosities are below 60%, a boundary that corresponds to the starting point for cementation in nannofossil oozes (Schlanger and Douglas, 1974).

ACKNOWLEDGMENTS

I thank the entire Leg 71 scientific and technical party for their cooperation aboard *Glomar Challenger*. Drs. G. Einsele, and A. Wetzel, Geologisches Institut der Universität Tübingen, and Drs. R. Flood, W. Ludwig, and A. Shor, Lamont-Doherty Geological Observatory, critically read the manuscript and made valuable comments.

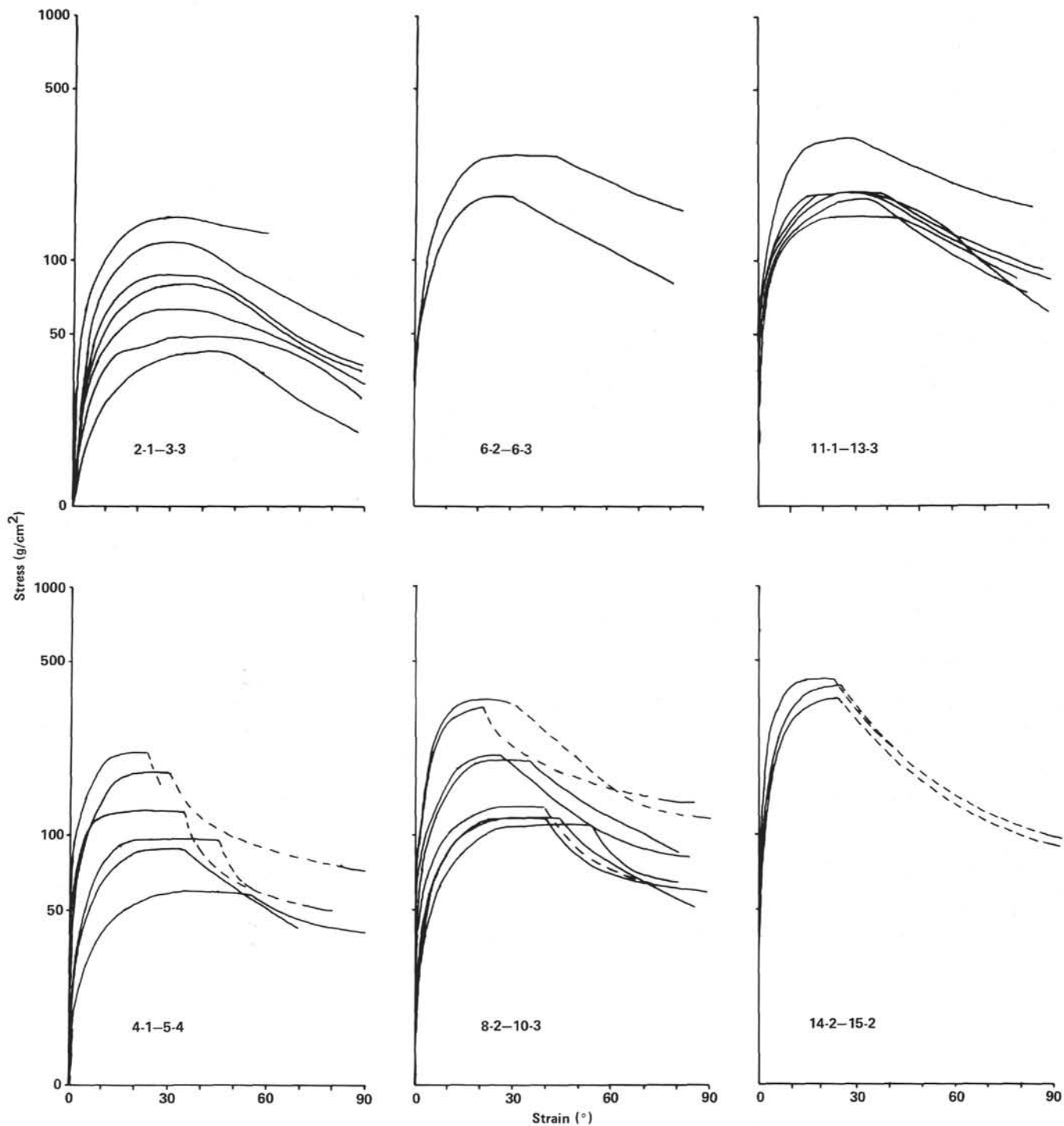


Figure 16. Stress-strain relations for Site 514. Data are grouped by topological patterns. Numbers on graphs indicate core and section interval. Dashed lines indicate areas where strain pointer moved too swiftly for data points to be recorded.

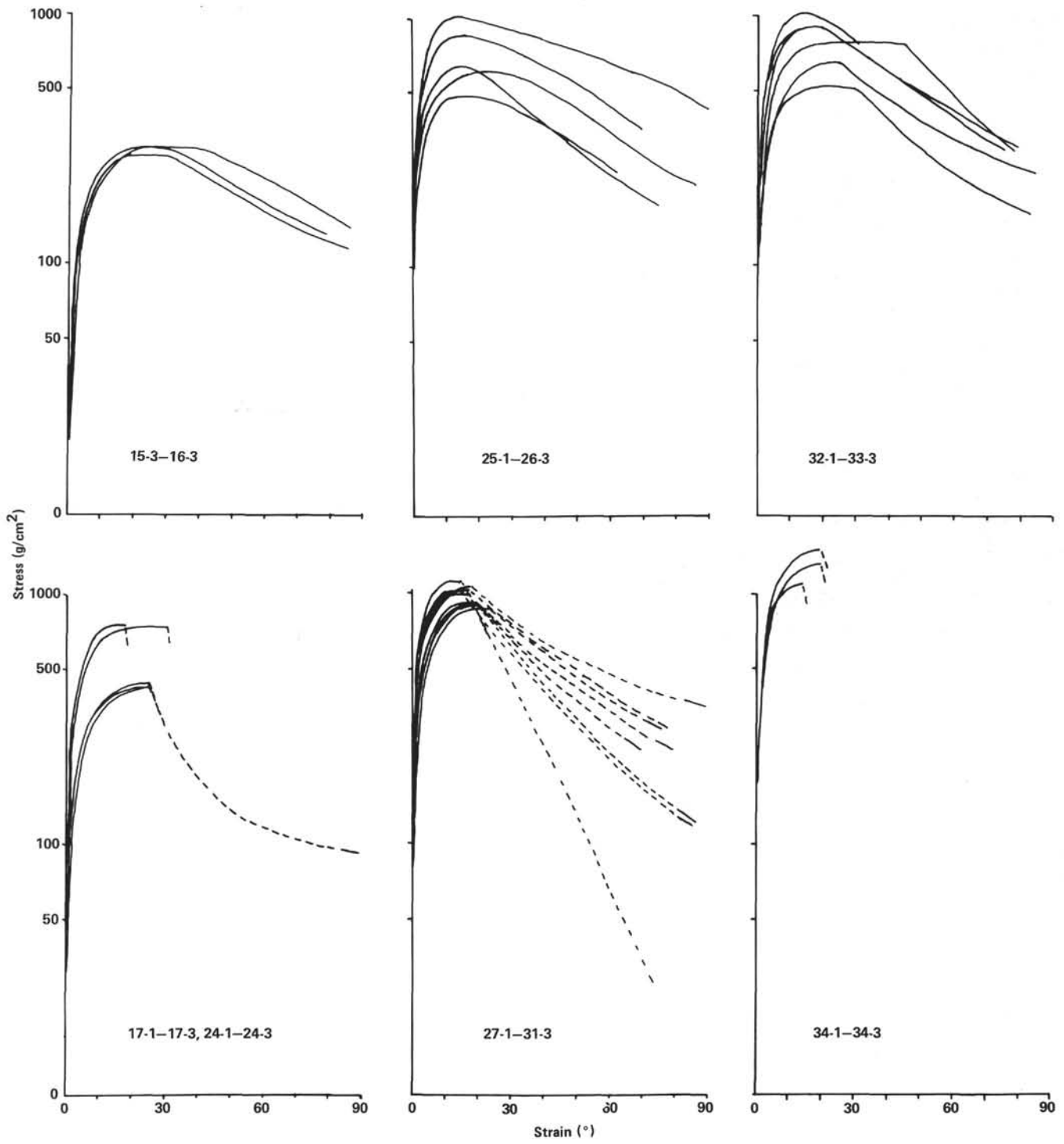


Figure 16. (Continued).

REFERENCES

- Bachman, R. T., and Hamilton, E. L., 1976. Density, porosity, and grain density of samples from Deep Sea Drilling Project Site 222 (Leg 23) in the Arabian Sea. *J. Sediment. Petrol.*, 46(no. 3): 654-658.
- Bennett, R. H., and Keller, G. H., 1973. Physical properties evaluation. In van Andel, Tj. H., Heath, G. R., et al., *Init. Repts. DSDP*, 16: Washington (U.S. Govt. Printing Office), 513-519.
- Boyce, R. E., 1976a. Definitions and laboratory techniques of compressional sound velocity parameters and wet-water content, wet-bulk density, and porosity parameters by gravimetric and gamma ray attenuation techniques. In Schlanger, S. O., Jackson, E. D., et al., *Init. Repts. DSDP*, 33: Washington (U.S. Govt. Printing Office), 931-958.
- , 1976b. Sound velocity-density parameters of sediment and rock from DSDP drill sites 315-318 on the Line Islands Chain, Manihiki Plateau, and Tuamotu Ridge in the Pacific Ocean. In Schlanger, S. O., Jackson, E. D., et al., *Init. Repts. DSDP*, 33: Washington (U.S. Govt. Printing Office), 695-728.
- , 1977. Deep Sea Drilling Project procedures for shear strength measurement of clayey sediment using modified Wykeham Farnance Laboratory Vane Apparatus. In Barker, P. F., Dalziel, I. W. D., et al., *Init. Repts. DSDP*, 36: Washington (U.S. Govt. Printing Office), 1059-1068.
- , 1980. Deep Sea Drilling Project Leg 50 laboratory physical-property methods. In Lancelot, Y., Winterer, E. L., et al., *Init. Repts. DSDP*, 50: Washington (U.S. Govt. Printing Office), 837-847.
- Calvert, S. E., 1974. Deposition and diagenesis of silica in marine sediments. *Spec. Publ. Int. Assoc. Sedimentol.*, 1:273-299.
- Demars, K. R., Nacci, V. A., Kelly, W. E., 1979. Engineering and other physical property data, Leg 43. In Tucholke, B. E., Vogt, P. R., et al., *Init. Repts. DSDP*, 43: Washington (U.S. Govt. Printing Office), 757-768.
- Einsele, G., 1982. Mass physical properties of Pliocene to Quaternary sediments in the Gulf of California (DSDP, Leg 64). In Curray, J. R., Moore, D. G., et al. *Init. Repts. DSDP*, 64: Washington (U.S. Govt. Printing Office), 529-542.
- Hamilton, E. L., 1976a. Variations of density and porosity with depth in deep-sea sediments. *J. Sediment. Petrol.*, 46:280-300.
- , 1976b. Shear-wave velocity versus depth in marine sediments: A review. *Geophysics*, 41(3):985-996.
- , 1976c. Attenuation of shear waves in marine sediments. *J. Acoust. Soc. Am.*, 60(2):334-338.
- , 1976d. Sound attenuation as a function of depth in the sea floor. *J. Acoust. Soc. Am.*, 50(3):528-535.
- , 1978. Sound velocity-density relations in sea-floor sediments and rocks. *J. Acoust. Soc. Am.*, 63(2):366-377.
- , 1979. Sound velocity gradients in marine sediments. *J. Acoust. Soc. Am.*, 65(4):909-922.
- Keller, G. H., 1974. Marine geotechnical properties: Interrelationships and relationships to depth of burial. In Inderbitzen, A. L. (Ed.), *Deep Sea Sediments*: New York (Plenum Press), pp. 77-100.
- Lee, H. J., 1973. Measurements and estimates of engineering and other physical properties, Leg 19. In Creager, J. S., Scholl, D. W., et al., *Init. Repts. DSDP*, 19: Washington (U.S. Govt. Printing Office), 701-719.
- Nacci, V. A., Wang, M. C., and Gallagher, J., 1974. Influence of anisotropy and soil structure on elastic properties of sediments. In Hampton, L. (Ed.), *Marine Science (Vol. 1) Physics of Sound in Marine Sediments*: New York (Plenum Press), pp. 63-87.
- Richards, A. F., Hirst, T. J., and Parks, J. M., 1974. Bulk density-water content relationship in marine silts and clays. *J. Sediment. Petrol.*, 44(no. 4):1004-1009.
- Schlanger, S. O., and Douglas, R. G., 1974. The pelagic ooze-chalk limestone transition and its implications for marine stratigraphy. *Spec. Publ. Int. Assoc. Sedimentol.*, 1:117-148.
- Sowers, C. F., 1979. *Introductory Soil Mechanics and Foundation* (4th ed.): New York (Macmillan).
- Stoll, R. D., 1974. Acoustic waves in saturated sediments. In Hampton, L. (Ed.), *Marine Science (Vol. 1) Physics of Sound in Marine Sediments*: New York (Plenum Press), 19-39.
- Taylor Smith, D., 1974. Acoustic and mechanical loading of marine sediments. In Hampton, L. (Ed.), *Marine Science (Vol. 1) Physics of Sound in Marine Sediments*: New York (Plenum Press), 41-61.
- Terzaghi, K., 1943. *Theoretical Soil Mechanics*: New York (John Wiley).
- von Huene, R., Piper, D. J. W., and Duncan, J., 1973. Measurements of porosity in sediments of the lower continental margin, deep-sea fans, the Aleutian trench, and Alaskan abyssal plain. In Kulm, L. D., von Huene, R., et al., *Init. Repts. DSDP*, 18: Washington (U.S. Govt. Printing Office), 889-895.
- Wyllie, M. R. J., Gregory, A. R., and Gardner, G. H. F., 1958. An experimental investigation of factors affecting elastic velocities in porous media. *Geophysics*, 23:459-493.

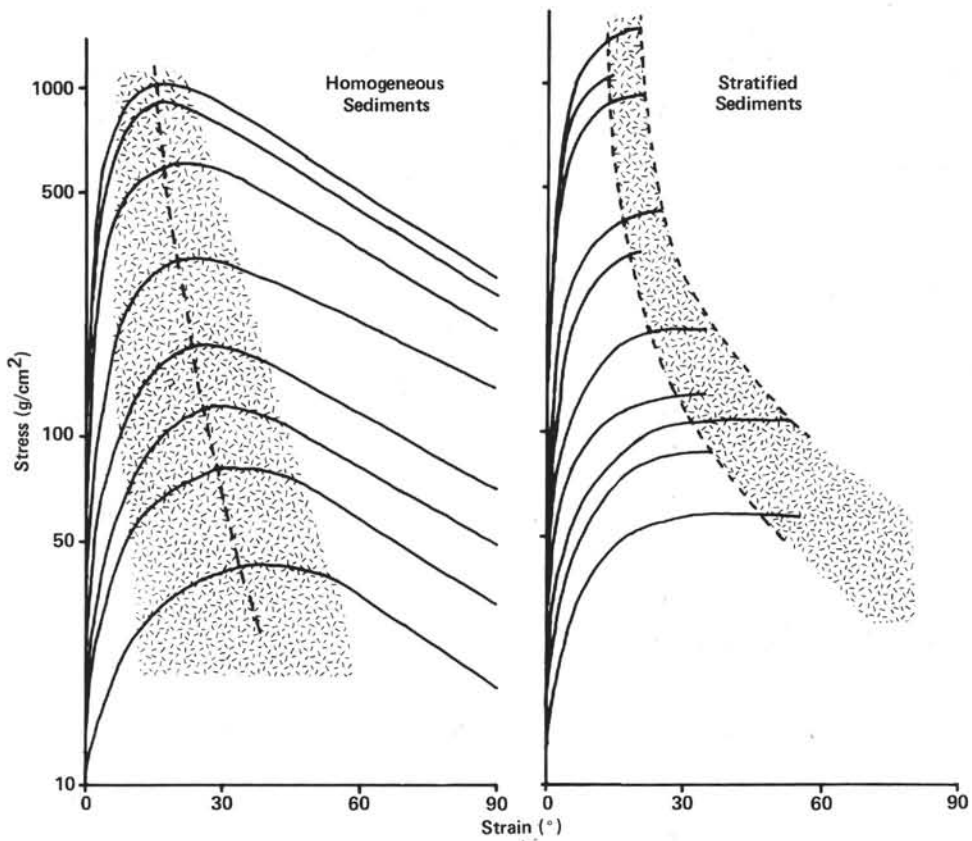


Figure 17. Summary of the qualitative stress-strain behavior of the diatomaceous oozes and muds of Site 514. Data are given separately for homogeneous (isotropic?) and stratified (anisotropic) sediments. Dashed lines indicate areas where strain pointer moved too swiftly for data points to be recorded.

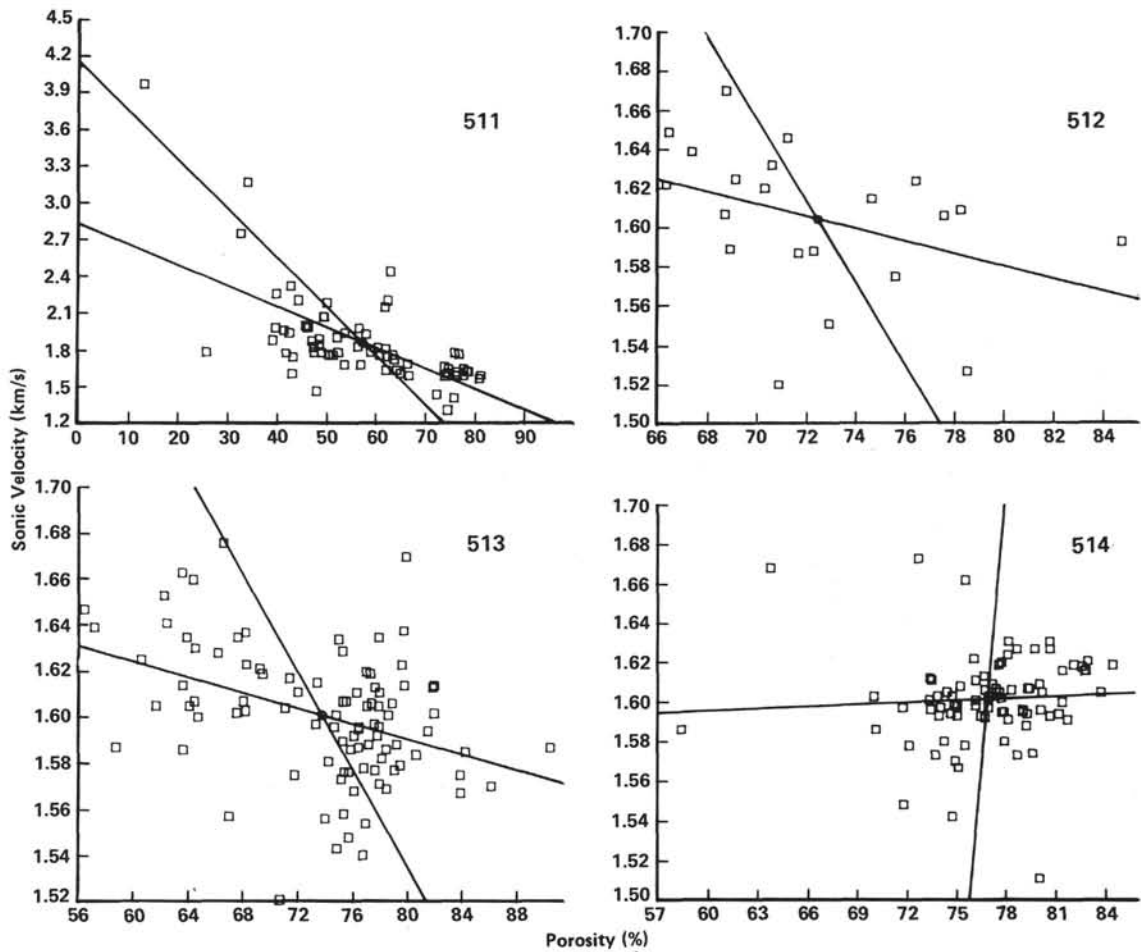


Figure 18. Linear relationship between sonic velocity and porosity from original data, Sites 511–514. For regression equations, see Table 8.

Table 8. Relationship between sonic velocity (V , in km/s) and porosity (ϕ).^a

Site	Regression Equation	N	r^2
511	$V = -1.688 \phi + 2.826$ $\phi = -0.25 V + 1.036$	73	0.42
512	$V = -0.317 \phi + 1.834$ $\phi = -0.478 V + 1.491$	21	0.15
513	$V = -0.169 \phi + 1.726$ $\phi = -0.944 V + 2.248$	95	0.16
514	$V = -0.038 \phi + 1.573$ $\phi = -0.112 V + 0.59$	80	0.004

^a Estimated from original data.

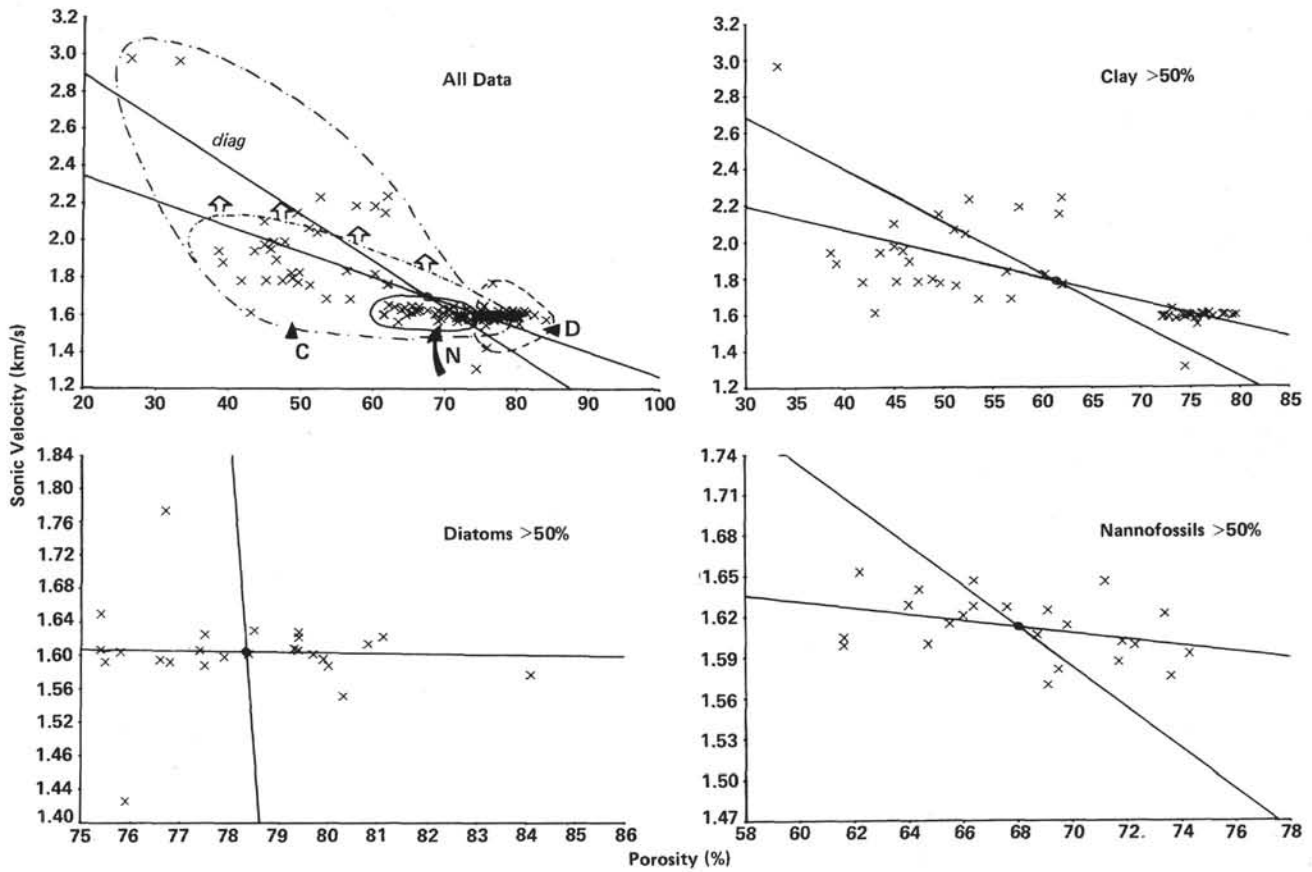


Figure 19. Linear relationship between sonic velocity and porosity for mean values of cores: all data, and sediments grouped by primary components (diag = area of diagenetic alteration). For regression equations, see Table 9.

Table 9. Relationship between sonic velocity (V , in km/s) and porosity (ϕ) for sediments grouped by primary components.^a

Condition	Regression Equation	N	r^2
Data for all sites	$V = -1.351 \phi + 2.616$ $\phi = -0.4 V + 1.36$	129	0.54
Sediment group			
Clay content >50%	$V = -1.31 \phi + 2.59$ $\phi = -0.35 V + 1.24$	51	0.46
Diatom content >50%	$V = -0.08 \phi + 1.67$ $\phi = -0.013 V + 0.8$	25	0.001
Nannofossil content >50%	$V = -0.231 \phi + 1.769$ $\phi = -0.667 V + 1.755$	23	0.15

^a Data are mean values for the cores.

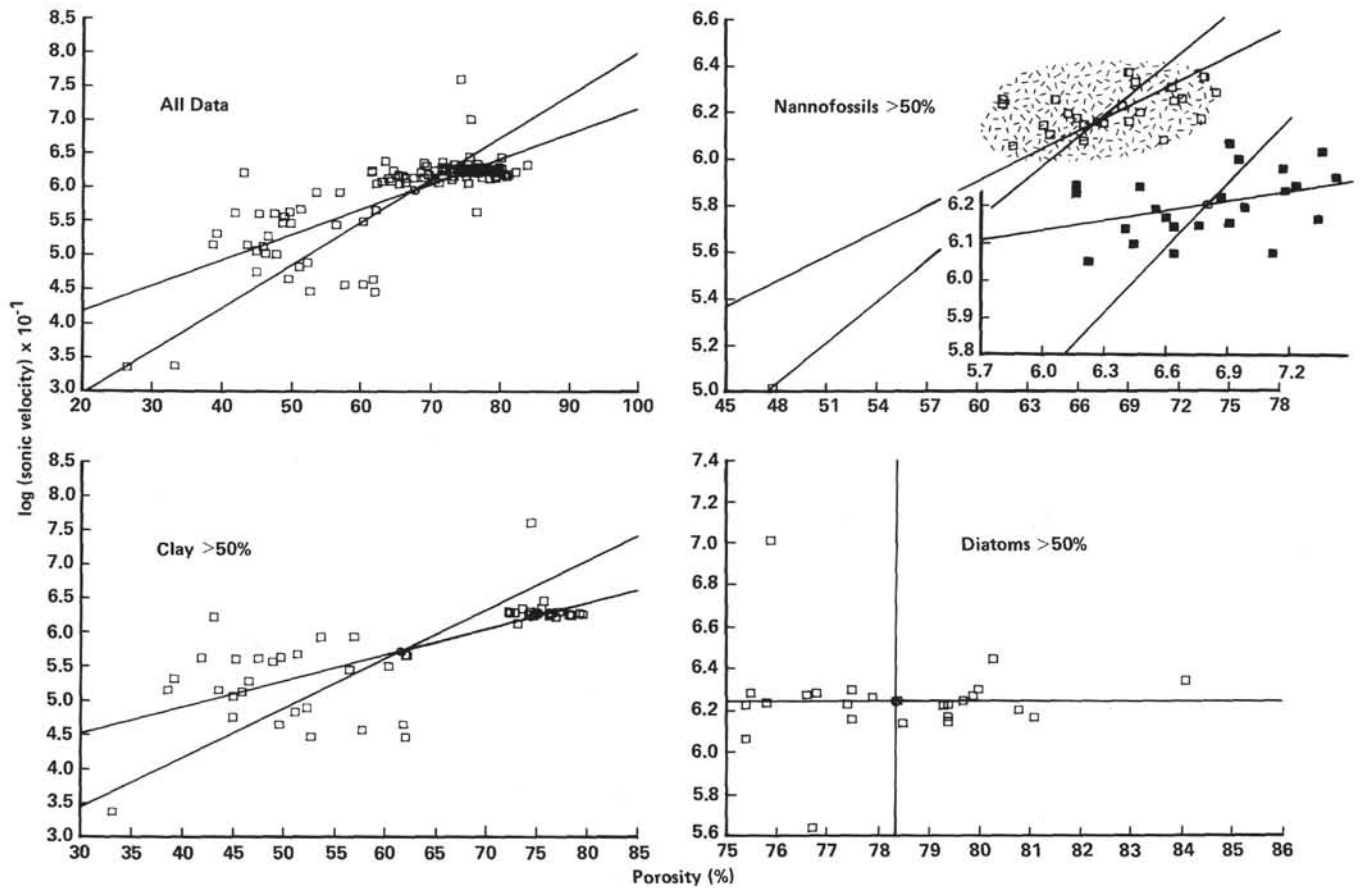


Figure 20. "Time average" relation between 1/(sonic velocity) and porosity for mean values of cores: all data, and sediments grouped by primary components. For regression equations, see Table 10.

Table 10. Relationship between sonic velocity (V) and porosity (ϕ) by the "time average formula."^a

Condition	Equation	V_s	V_f	N	r^2
Data for all sites	$\frac{1}{V} = 0.376 \phi + 0.341$ $\phi = 1.585 / V - 0.267$	2.93	1.39	129	0.596
Sediments grouped by primary components					
Clay content > 50%	$\frac{1}{V} = 0.383 \phi + 0.335$ $\phi = 1.382 / V - 0.174$	2.98	1.39	51	0.53
Diatom content > 50%	$\frac{1}{V} = 0.004 \phi + 0.62$ $\phi = 0.004 / V - 0.78$	1.61	1.60	25	0.0
Nannofossil content > 50%	$\frac{1}{V} = 0.356 \phi + 0.376$ $\phi = 1.7 / V - 0.38$	2.66	1.37	24	0.61
Data corrected for 1 extreme point	$\frac{1}{V} = 0.09 \phi + 0.56$ $\phi = 1.73 / V - 0.39$	1.79	1.50	23	0.15

^a Data are mean values for cores.